

Spatial optimal growth in three-dimensional boundary layers

DAVID TEMPELMANN¹, ARDESHIR HANIFI^{1,2†}
AND DAN S. HENNINGSON¹

¹Linné Flow Centre, KTH Mechanics, SE-100 44 Stockholm, Sweden

²Swedish Defence Research Agency, FOI, SE-164 90 Stockholm, Sweden

(Received 7 May 2009; revised 3 November 2009; accepted 4 November 2009)

A parabolized set of linear equations is derived, which, in combination with the proposed solution procedure, allows for the study of both non-modal and modal disturbance growth in three-dimensional boundary layers. The method is applicable to disturbance waves whose lines of constant phase are closely aligned with the external streamline. Moreover, strongly growing disturbances may fall outside the scope of application. These equations are used in conjunction with a variational approach to compute optimal disturbances in Falkner–Skan–Cooke boundary layers subject to adverse and favourable pressure gradients. The disturbances associated with maximum energy growth initially take the form of streamwise vortices which are tilted against the mean crossflow shear. While travelling downstream these vortical structures rise into an upright position and evolve into bent streaks. The physical mechanism responsible for non-modal growth in three-dimensional boundary layers is therefore identified as a combination of the lift-up effect and the Orr mechanism. Optimal disturbances smoothly evolve into crossflow modes when entering the supercritical domain of the flow. Non-modal growth is thus found to initiate modal instabilities in three-dimensional boundary layers. Optimal growth is first studied for stationary disturbances. Influences of parameters such as sweep angle, spanwise wavenumber and position of inception are studied, and the initial optimal amplification of stationary crossflow modes because of non-modal growth is investigated. Finally, general disturbances are considered, and envelopes yielding the maximum growth at each position are computed. In general, substantial growth is already found upstream of the first neutral point. The computations show that at supercritical conditions, maximum growth of optimal disturbances in accelerated boundary layers can exceed the growth predicted for modal instabilities by several orders of magnitude.

1. Introduction

The classical approach to transition prediction is based on exponential amplification of discrete modes. This so-called modal growth serves as an input for prediction methods such as the well-known e^N -method, which then provide a certain location for transition from laminar to turbulent flow. Modal growth is often computed locally under the assumption of a parallel baseflow by solving the Orr–Sommerfeld equation. More advanced non-local methods were developed for convectively unstable flows by Herbert and Bertolotti and by Dallmann and Simen (see e.g. Bertolotti, Herbert

† Email address for correspondence: ardeshir.hanifi@foi.se

& Spalart 1992; Simen 1992), allowing for non-parallel baseflows. Both approaches are based on parabolizing the linear stability equations and only differ with respect to the order of which terms are kept. We will commonly refer to these methods as the classical parabolized stability equations (PSEs). They were found to correctly reproduce modal growth in two- and three-dimensional boundary layers (see e.g. Bertolotti *et al.* 1992; Hanifi *et al.* 1994; Herbert 1997; Bippes 1999; Saric, Reed & White 2003).

It is known that the external conditions, i.e. free-stream turbulence and surface roughness, have a large influence on the disturbance development. Deyhle & Bippes (1996) performed several experiments on three-dimensional boundary layers in different wind tunnels. They observed a strong dependence of the disturbance development on upstream conditions. Bippes (1999) has summarized that the changes in the disturbance development are quite dramatic. At low free-stream turbulence levels stationary crossflow modes dominate, whereas at high levels travelling modes become more energetic. These findings have been confirmed numerically by Schrader, Brandt & Henningson (2009) and Schrader, Amin & Brandt (2010). Therefore it is important to include the initiation of modal disturbances within the boundary layer, the so-called receptivity process, in transition prediction tools. Schrader *et al.* (2009) studied the receptivity to both free-stream vorticity and surface roughness in a three-dimensional swept-plate boundary layer by means of direct numerical simulation (DNS). They showed that the receptivity coefficient which determines the initial amplification varies for individual crossflow modes of different wavenumbers and frequencies. Furthermore the position at which the external disturbance impinges has an influence on the receptivity. The numerical simulations by Schrader *et al.* (2010) have shown that for high levels of free-stream turbulence the initial disturbance development is characterized by non-modal growth of streak-like disturbances which then evolve into unsteady crossflow modes. Hence, non-modal growth can be related to a receptivity mechanism initiating modal instabilities in three-dimensional boundary layers. Optimal disturbances, being maximally amplified, can therefore be used to determine the maximum possible initial amplification of crossflow modes.

1.1. *Non-modal growth in two-dimensional boundary layers*

Non-modal growth and optimal disturbances have been studied extensively for two-dimensional boundary layers. Ellingsen & Palm (1975) demonstrated that three-dimensional streaky disturbances can be amplified linearly in inviscid channel flow. Hultgren & Gustavsson (1981) found these disturbances to be present in viscous flow where they eventually decay because of viscous dissipation, leading to the term ‘transient’ growth. A physical explanation for this non-modal growth mechanism which is commonly known as the ‘lift-up’ effect has been given by Landahl (1980). Fluid particles keeping their horizontal momentum when being vertically displaced because of streamwise vortices lead to the formation of streamwise-elongated structures. These have been found to initiate transition in a number of experiments on boundary layers subject to free-stream turbulence by e.g. Klebanoff (1971), Kendall (1985) and Matsubara & Alfredsson (2001). The fact that this transition scenario does not build on exponentially growing Tollmien–Schlichting (TS) waves led to the expression ‘bypass’ transition. Transient growth has been the subject of numerous theoretical and numerical studies in the temporal framework for various parallel incompressible flows, most notably those by Butler & Farrell (1992), Henningson, Lundbladh & Johansson (1993), Reddy & Henningson (1993) and Corbett & Bottaro

(2000). Mathematically, non-modal growth can be explained to be due to the non-normality of the governing linear operator as outlined in Schmid & Henningson (2001). However, because boundary layers represent convectively unstable flows it is physically more relevant to study disturbance growth within the spatial framework. Andersson, Berggren & Henningson (1999) and Luchini (2000) were the first to study spatial optimal growth in the non-parallel Blasius boundary layer. Both studies have shown that in the high-Reynolds-number limit global optimal growth scales linearly with the Reynolds number and is obtained for stationary disturbances. The work on non-modal as well as modal growth by Levin & Henningson (2003) has revealed that these two growth mechanisms compete in two-dimensional boundary layers and become dominant for different values regarding spanwise wavenumber and frequency.

Extending the study to two-dimensional compressible boundary layers similar effects as those outlined above have been found by Hanifi, Schmid & Henningson (1996) who employed a temporal framework and by Tumin & Reshotko (2003) who used a spatial approach.

Besides the lift-up effect a second non-modal growth mechanism was shown to exist by Butler & Farrell (1992). This effect builds on the action of a perturbation Reynolds stress and is referred to as the Orr mechanism (Orr 1907). Structures which are tilted against the mean shear gain energy from the meanflow while being erected. Eventually the energy is returned to the meanflow, and the disturbances decay. This two-dimensional mechanism has been found to optimally initiate TS waves by Åkervik *et al.* (2008). However, in the Blasius boundary layer this non-modal growth mechanism is much weaker compared with the lift-up effect.

1.2. Non-modal growth in three-dimensional boundary layers

Unlike for two-dimensional boundary layers not much work on non-modal growth has been done concerning their three-dimensional counterparts. Breuer & Kuraishi (1994) and Corbett & Bottaro (2001) who studied non-modal growth in three-dimensional boundary layers employing a temporal framework illuminated the principle difference. Both non-modal growth and modal growth are observed for similar disturbance structures, which is contrary to the two-dimensional case. Corbett & Bottaro (2001) who studied temporal optimal disturbances in three-dimensional boundary layers found that these initially take the form of vortices which are almost aligned with the external streamline and evolve into streaks. By comparing the output of non-modal growth with the most unstable eigenmode Corbett & Bottaro (2001) concluded that algebraic growth and exponential growth complement each other. They argued that non-modal growth may provide proper initial conditions for modal growth and thus constitutes a preferential receptivity path for the selection of exponential instabilities in three-dimensional boundary layers. A spatial framework is however needed to take into account non-parallel and non-local effects and to correctly describe the initiation of modal instabilities because of non-modal growth. Two approaches to obtain spatial optimal disturbances in three-dimensional boundary layers are presented in Pralits *et al.* (2007). The first one, termed single-mode approach, is based on the existence of one dominating mode. The optimal initial disturbance and with it a so-called amplification factor which determines the initial amplification of the dominating mode are then obtained on the basis of the adjoint solution of the corresponding modal instability. However, the initial non-modal growth of the optimal disturbance cannot be observed by employing this method, although its final amplification is captured correctly. Also, in stable regions in which it is difficult to

identify discrete modes amplification factors may not be yielded. The second approach (see also Byström 2007) is based upon a parabolized set of equations which are integrated along a curved line denoting the disturbance path. Hence, the downstream development of the initial disturbance is obtained for the entire domain. Optimal growth and the corresponding initial disturbance are then computed via adjoint-based optimization.

Herein we present a method which is related to the one by Byström (2007). We derive a parabolized set of equations governing the spatial linear evolution of an arbitrary initial disturbance in a non-parallel baseflow and present a method to solve them. Spatial optimal disturbances are then obtained by employing the method of Lagrange multipliers. In general, optimal growth is studied for boundary layers over a swept flat plate subject to an adverse as well as a favourable pressure gradient and for different sweep angles. When presenting results we first concentrate on optimal stationary disturbances. As outlined above, stationary disturbances are known to dominate in low-turbulence environments and are thus important in terms of transition prediction. We investigate the role non-modal growth plays with respect to the initiation of modal instabilities and discuss its physical mechanisms in three-dimensional boundary layers. Finally, the restriction of zero frequency is dropped, and the maximum growth that can be obtained along the chord of the flat plate is determined. This is achieved by combining the variational approach that provides the optimal disturbance shape with a Newton line search algorithm to obtain the corresponding optimal spanwise wavenumber, frequency and initial position at which the disturbance is introduced. This yields an envelope comprising non-modal growth.

2. Falkner–Skan–Cooke boundary layer

Throughout the current paper we will describe the evolution of disturbances in a boundary layer over a swept flat plate which is infinitely elongated in the spanwise direction and is subject to a chordwise pressure gradient. This type of boundary layer is often considered as a model for swept-wing boundary layers because it comprises two important features, namely a pressure gradient and a sweep angle. The resulting imbalance between pressure and centrifugal forces creates an inflectional profile of the crossflow velocity component, leading to an inviscid inflectional instability which provokes the amplification of the so-called crossflow vortices.

The three-dimensional boundary layer equations may be reduced for the infinite swept plate such that a solution for the chordwise and wall-normal velocities U and W is obtained from the corresponding two-dimensional equations. The spanwise velocity component V can then be determined subsequently from the equation, enforcing conservation of spanwise momentum. A self-similar solution to these equations, which is commonly known as the Falkner–Skan–Cooke (FSC) boundary layer (Cooke 1950), is obtained assuming the chordwise and spanwise velocities at the boundary layer edge, U_e and V_e , to obey

$$\frac{U_e}{Q_\infty} = \left(\frac{x}{l}\right)^m \quad \text{and} \quad \frac{V_e}{Q_\infty} = \sin \Lambda, \quad (2.1)$$

with $m = \beta_H/(2 - \beta_H)$, where β_H is the Hartree parameter (which specifies the pressure gradient). The subscript e denotes velocities at the boundary layer edge and l represents some characteristic length. The coordinate system, the velocities and the sweep angle

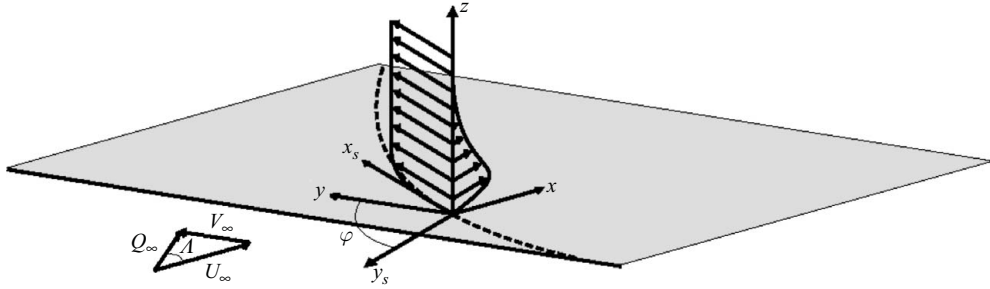


FIGURE 1. Sketch of the streamwise and the crossflow mean velocity components of an FSC boundary layer. The curved external streamline is indicated by the dashed line. The coordinates (x, y, z) denote the chordwise, spanwise and wall-normal directions, whereas (x_s, y_s, z) refer to the streamwise, crossflow and wall-normal directions. The velocity components (U, V, W) as well as (U_s, V_s, W) are defined respectively; Q_∞ is the incoming total velocity; Λ represents the sweep angle and $\varphi = \varphi(x)$ denotes the angle between the streamwise and the chordwise direction at each chordwise position x .

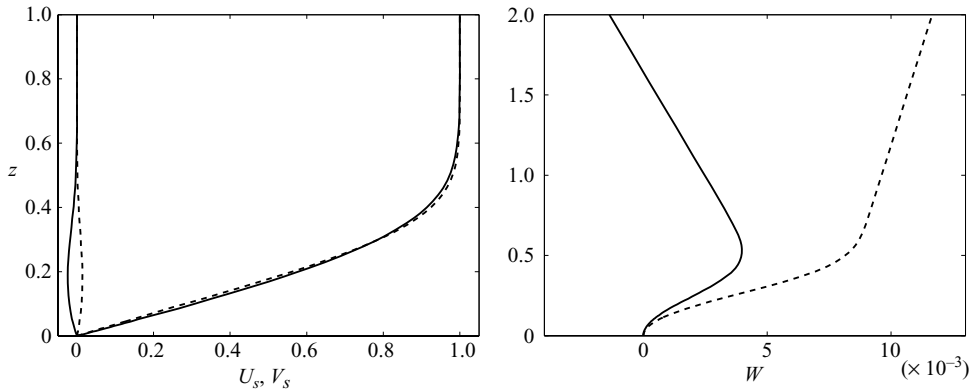


FIGURE 2. FSC solutions for Hartree parameters $\beta_H = 0.1$ (—) and $\beta_H = -0.05$ (---) at $x/l = 0.01$. The sweep angle is $\Lambda = 45^\circ$. The velocity components denoted by the subscript s were projected on to the streamwise and the crossflow direction respectively.

Λ are defined in figure 1. Assuming (2.1) would allow the reduction of the boundary layer equations further to a function of one single similarity variable. However, we obtain the FSC solutions U , V and W by solving the above-described quasi-three-dimensional boundary layer equations. The projection on to the streamwise and the crossflow direction respectively yields

$$U_s = U \cos \varphi + V \sin \varphi, \quad (2.2)$$

$$V_s = -U \sin \varphi + V \cos \varphi. \quad (2.3)$$

Velocities (2.2) and (2.3) as well as the wall-normal velocity component are shown in figure 2, where z is normalized with the reference length $\delta = \sqrt{\nu l / Q_l}$; Q_l is the total mean velocity in the free stream at $x = l$ and ν represents the kinematic viscosity. For further details, the reader is referred to Schlichting (1979).

3. Methodology

3.1. Governing equations

Our aim is to describe the spatial evolution of three-dimensional disturbances in an FSC boundary layer. To be able to obtain spatial optimal disturbances and to perform parametric studies we would like to arrive at a linear and parabolic set of equations which can be easily solved numerically, using marching techniques. To this end one could consider the use of the well-known PSEs (see e.g. Bertolotti *et al.* 1992; Simen 1992; Herbert 1997) which have been successfully used to compute the exponential growth of three-dimensional disturbances in an FSC boundary layer by e.g. Högberg & Henningson (1998). However, the PSEs as they are commonly used are not capable of predicting non-modal growth of disturbances. This is because the PSEs are limited to describing the exponential growth of one particular mode, whereas non-modal growth is known to result from the superposition of exponentially growing or decaying modes. In the following we will modify the classical PSE method and make it capable of accounting for both modal and non-modal growth. As for the classical PSEs we start our derivation with the incompressible Navier–Stokes equations

$$\nabla \cdot \mathbf{u} = 0, \quad (3.1a)$$

$$\frac{\partial \mathbf{u}}{\partial t} + (\mathbf{u} \cdot \nabla) \mathbf{u} = -\frac{1}{\rho} \nabla P + \nu \nabla^2 \mathbf{u}. \quad (3.1b)$$

Here, P represents the pressure, ρ the density and \mathbf{u} the velocity vector. Decomposing these quantities into a mean and a perturbation part, subtracting the equations governing the meanflow and linearizing the resulting equation by neglecting all products of perturbation quantities yields

$$\nabla \cdot \mathbf{u}' = 0, \quad (3.2a)$$

$$\frac{\partial \mathbf{u}'}{\partial t} + (\mathbf{u}' \cdot \nabla) \mathbf{U} + (\mathbf{U} \cdot \nabla) \mathbf{u}' = -\frac{1}{\rho} \nabla p' + \nu \nabla^2 \mathbf{u}', \quad (3.2b)$$

where mean quantities are represented by upper-case letters and $'$ denotes perturbation quantities. Still following the derivation of the classical PSEs we consider flows which are homogeneous in the spanwise direction. We thus define the disturbances to take the form

$$\mathbf{q}'(x, y, z, t) = \mathbf{q}(x, z) \exp i\Theta(x, y, t), \quad (3.3)$$

$$\Theta(x, y, t) = \int_{x_0}^x \alpha(x') dx' + \beta y - \omega t, \quad (3.4)$$

where β represents the spanwise wavenumber, α the chordwise wavenumber and ω the angular frequency and $\mathbf{q} = (u, v, w, p)^T$. Both the shape function $\mathbf{q}(x, z)$ in (3.3) and the chordwise wavenumber in (3.4), which is assumed to be complex in the classical PSE approach, are functions of x . This ambiguity is usually resolved by means of an auxiliary condition of the form

$$\int_0^\infty \mathbf{q}^H \frac{\partial \mathbf{q}}{\partial x} dz = 0, \quad (3.5)$$

where the superscript H denotes complex conjugate transpose. Condition (3.5) represents a normalization on the shape function and ensures that the growth and the chordwise periodic variation of the disturbance are mainly absorbed by the

	x	z	U, V	W	u, v	w	α	β	p	t	ω
BL scaling	l	δ	Q_l	$Q_l \delta / l$	Q_l	$Q_l \delta / l$	$1/\delta$	$1/\delta$	$\rho Q_l^2 \delta / l$	l/Q_l	Q_l/l
PSE scaling	l	δ	Q_l	$Q_l \delta / l$	Q_l	Q_l	$1/\delta$	$1/\delta$	ρQ_l^2	δ/Q_l	Q_l/δ

TABLE 1. Scales assumed for the variables of (3.2) based on the boundary layer as well as the PSE approximation; BL stands for boundary layer.

exponential part of (3.3). This allows for the assumption of a slow variation of $\mathbf{q}(x, z)$ in the chordwise direction x . However, together with the common approach of taking a local eigenmode as an initial disturbance it also constitutes a reason why the PSEs are restricted to the prediction of modal growth. Thus, to be able to account for non-modal growth we omit the auxiliary condition and resolve the above-described ambiguity by prescribing the chordwise wavenumber $\alpha(x)$ as a real function based on lines of constant phase. This approach is described in §3.2 and assures that the chordwise periodic variation of the disturbance is taken care of by the exponential part of (3.3). The growth of \mathbf{q}' is then completely absorbed by the shape function.

In the next step we compare the relative order of the different terms of (3.2) in order to identify those which are negligible and to finally arrive at a parabolized set of equations. The problem comprises two characteristic length scales, namely a typical length scale l in the chordwise direction and $\delta = \sqrt{\nu l / Q_l}$, where $\delta \ll l$, in the wall-normal direction. Hence, to determine the relative order of all terms in (3.2) we need to scale them appropriately. Andersson *et al.* (1999) and Luchini (2000) chose a scaling based on the boundary layer approximation to study non-modal growth of streaks in a Blasius boundary layer. Levin & Henningson (2003) extended the study to Falkner–Skan boundary layers and included the terms originating from the PSE scaling to also account for exponentially growing disturbances. Bagheri & Hanifi (2007) used the same approach to study the stabilizing effect of streaks on modal instabilities in a Blasius boundary layer. Their results were in close agreement with the DNS. The PSE scaling is based on the assumption that the gradients in the wall-normal and the wall-tangential direction of both the amplitude functions (3.3) and the phase function (3.4) are of the same relative order as the gradients of the steady boundary layer flow. Except for the wall-normal meanflow component W which is assumed to be $O(Re_\delta^{-1})$ all other meanflow and disturbance quantities U, V, \mathbf{q} are considered as $O(1)$ in (3.2), where $Re_\delta = Q_l \delta / \nu = l / \delta$ (see Simen 1992; Schmid & Henningson 2001).

We follow the approach by Levin & Henningson (2003), since we need to consider modal as well as non-modal growth. Therefore the PSE scaling and a scaling based on the boundary layer approximation (both presented in table 1) are applied to the disturbance equations (3.2). Only those terms which are of orders higher than Re_δ^{-1} with respect to both scalings are neglected. This yields a composite approximation valid for modal and non-modal growth. Both scalings imply a slow variation of the shape function $\mathbf{q}(x, z)$ along the chordwise direction x . However, since the growth is completely absorbed by the shape function the assumption of slow variation may not be correct for disturbances exhibiting strong exponential growth. Therefore, the applicability of this method is limited to flows comprising non-modal and moderate exponential growth. Collecting terms $O(1)$ and $O(Re_\delta^{-1})$ and making them

non-dimensional using some reference quantities u_{ref}, l_{ref} results in

$$0 = u_x + i\alpha u + i\beta v + w_z, \quad (3.6a)$$

$$0 = -i\omega u + uU_x + wU_z + Uu_x + U i\alpha u + V i\beta u + W u_z \\ (+p_x) + i\alpha p + \frac{1}{Re}(\alpha^2 u + \beta^2 u - u_{zz}), \quad (3.6b)$$

$$0 = -i\omega v + uV_x + wV_z + Uv_x + U i\alpha v + V i\beta v + W v_z \\ + i\beta p + \frac{1}{Re}(\alpha^2 v + \beta^2 v - v_{zz}), \quad (3.6c)$$

$$0 = -i\omega w + uW_x + wW_z + Uw_x + U i\alpha w + V i\beta w + W w_z \\ + p_z + \frac{1}{Re}(\alpha^2 w + \beta^2 w - w_{zz}), \quad (3.6d)$$

where the subscripts denote partial derivatives and $Re = u_{ref} l_{ref} / \nu$. However, these equations are only quasi-parabolic. They exhibit an inherent ellipticity which can cause numerical instabilities at small Δx (see e.g. Li & Malik 1996, 1997; Andersson, Henningson & Hanifi 1998). In order to relax this numerical instability we need to omit the disturbance pressure gradient p_x in the chordwise momentum equation (3.6b) as was proposed by Haj-Hariri (1994) for the classical PSEs. It should be noted that this is not justified by the above analysis, since p_x is of higher order only with respect to the boundary layer scaling. However, by comparing with the results from the DNSs in §4.1 we find that in FSC boundary layers, p_x has only negligible effects on the computed results. The uW_x term in the wall-normal momentum equation (3.6d) is the only term originating from the boundary layer scaling, which is of higher order with respect to the PSE scaling. It was therefore found to be important for non-modal growth by Bagheri & Hanifi (2007).

Equations (3.6) pose an initial-value problem. Introducing an initial disturbance $\mathbf{q}(x_0)$ a marching procedure may be adopted to yield the downstream development of the initial disturbance, while we are interested in solutions subject to boundary conditions

$$u = v = w = 0 \quad \text{at} \quad z = 0, \quad (3.7a)$$

$$u \rightarrow 0, \quad v \rightarrow 0, \quad w \rightarrow 0 \quad \text{as} \quad z \rightarrow \infty. \quad (3.7b)$$

Equations (3.6) can be expressed in compact operator form as

$$\mathbf{L}\mathbf{q} = 0 \quad (3.8)$$

with \mathbf{L} being a linear operator of the form

$$\mathbf{L} = \mathbf{A} + \mathbf{B} \frac{\partial}{\partial z} + \mathbf{C} \frac{\partial^2}{\partial z^2} + \mathbf{D} \frac{\partial}{\partial x}. \quad (3.9)$$

The operators \mathbf{A} , \mathbf{B} , \mathbf{C} and \mathbf{D} are defined in Appendix A.

3.2. Determining the chordwise wavenumber α

Our intention is to determine the chordwise wavenumber α such that the periodic variations of the disturbances are captured by the exponential part of (3.3). The propagation direction of a wave is denoted by the wave vector \mathbf{k} shown in figure 3. Knowing the direction of \mathbf{k} specified by the angle ϕ and the spanwise wavenumber β we can determine the chordwise wavenumber α of the disturbance wave according to

$$\alpha(x) = -\tan(\phi(x))\beta. \quad (3.10)$$

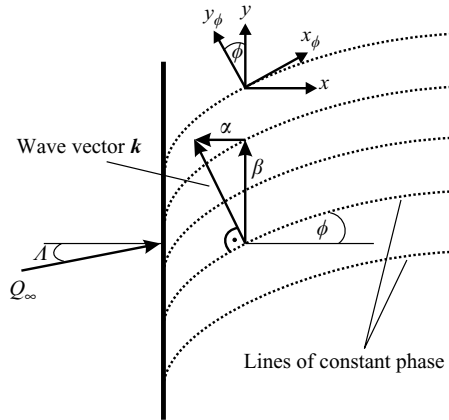


FIGURE 3. Illustration showing lines of constant phase and the dependence of the chordwise wavenumber α on both the angle ϕ and the spanwise wavenumber β . A coordinate system (x_ϕ, y_ϕ) is introduced, where x_ϕ denotes a direction tangential to the lines of constant phase. The corresponding velocity components are (u_ϕ, v_ϕ) .

The wave vector and accordingly the propagation direction of a disturbance wave are generally not known beforehand. Yet we know that the propagation direction is perpendicular to the line of constant phase whose trajectory (x, y) is related to ϕ through

$$\frac{\partial y}{\partial x} = \tan(\phi(x)) \quad (3.11)$$

and which, for low-frequency disturbances, is closely aligned to the external streamline in three-dimensional boundary layers (see Bippes 1999). However, the lines of constant phase of different flow quantities, e.g. (u, v, w, p) , are not identical because each respective complex shape function will add a different phase shift to the phase function (3.4). In order to obtain a well-defined chordwise wavenumber α it needs to be determined on the basis of the line of constant phase of one specific quantity. Here we choose it to be the disturbance velocity component containing most of the disturbance energy. This way we ensure that the largest variations because of oscillatory motion in the chordwise direction are captured by the wavenumber α . We know from Corbett & Bottaro (2001) that optimal disturbances will evolve from streamwise-oriented vortical structures into bent streaks and eventually into crossflow modes in three-dimensional boundary layers. Because streaks as well as low-frequency crossflow modes are mainly characterized by disturbance motion perpendicular to their wave vector \mathbf{k} it is the velocity component u_ϕ (see figure 3 for definition) that contains most of the disturbance energy. In the following we will therefore determine α on the basis of the line of constant phase of u_ϕ . Since u_ϕ and ϕ are not known beforehand and directly depend on each other they need to be determined iteratively.

It is only in a region very close to the initial position x_0 that u_ϕ does not represent the most energetic flow quantity. Here the initial vortical structures evolve into streaks, and thus the lines of constant phase based on any flow quantity are varying rapidly. We define this initial region to range from x_0 to a chordwise position x_i at which the major part of the disturbance energy is concentrated in u_ϕ . Hence, x_i denotes the position at which streak-like disturbances become the dominating structure. The actual definition of x_i can be found in figure 4. We therefore choose ϕ to be constant

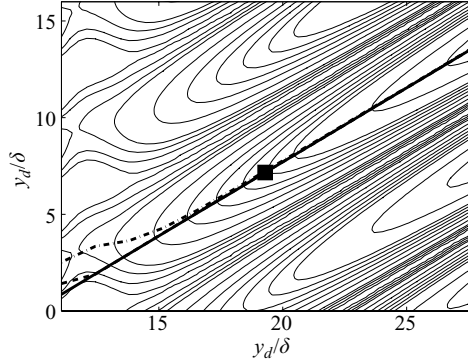


FIGURE 4. Contours of disturbance energy of optimal disturbance for $\beta_d \times \delta = 0.55$, $\omega = 0$, $\beta_H = 0.1$, $\Lambda = 45^\circ$ and $x_{0,d}/l = 0.01$. The wall-normal position of maximum energy is considered at each chordwise position. Lines of constant phase based on maximum disturbance energy (---) as well as the maximum of u_ϕ (---) are shown. Where both are close to each other, meaning $|y_E - y_{u_\phi}| / \max(y_E, y_{u_\phi}) < \epsilon$ the streak is assumed to be well defined; ϵ is usually taken between 0.01 and 0.001. The corresponding position x_i is denoted by \blacksquare . The solid line (—) represents the line chosen for the computations, which is identical to (---) for $x \geq x_i$ and is based on a constant $\phi = \phi(x_i)$ upstream of x_i . The subscript d denotes dimensional quantities.

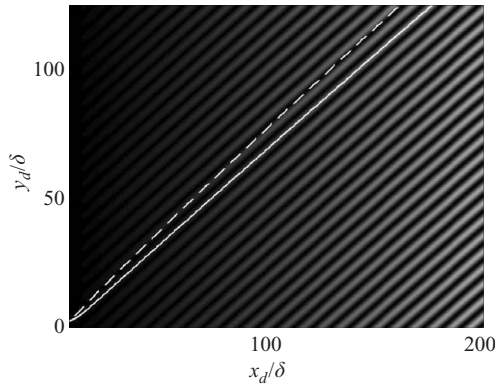


FIGURE 5. Visualization of energy of optimal disturbances for $\beta_d \times \delta = 0.55$, $\beta_H = 0.1$, $\Lambda = 45^\circ$ and $x_{0,d}/l = 0.01$. The solid white line (—) denotes a line of constant phase of u_ϕ as shown in figure 4, whereas the dashed line (---) represents the external streamline. The subscript d denotes dimensional quantities.

as $\phi = \phi(x_i)$ for $x < x_i$, whereas ϕ is based on the line of constant phase of $\max_z(u_\phi)$ for $x \geq x_i$.

The governing equations (3.8) are solved in an iterative manner. During the first iteration step the external streamline together with $u_\phi = u_s$ is used to determine ϕ and α and $\phi = \varphi$. On the basis of the lines of constant phase of that first solution u_ϕ , α and ϕ are updated and are then used to solve (3.8) in the next iteration step. The two latter steps are repeated until the energy growth has converged. For the cases we consider in the following, three to five iterations have usually been sufficient.

The line of constant phase based on u_ϕ is indeed closely aligned with the external streamline as can be seen in figure 5. However, basing our computations solely upon the external streamline leads to small errors locally, which then accumulate while

integrating downstream. All results presented in the following are therefore computed employing the iterative procedure outlined above.

It should be noted that the line of constant phase can also be identified as a disturbance or ray path along which the disturbance travels downstream. In light of this the method presented here is related to the one by Byström (2007), who derived a parabolic set of compressible equations using non-orthogonal, curvilinear coordinates where the curved coordinate was chosen to follow the disturbance path. Transforming those equations back to Cartesian coordinates, introducing a chordwise wavenumber according to (3.10) and considering the incompressible limit will result in (3.6). Another related method is based on complex-ray theory, which was applied to flow instabilities in boundary layers by Gréa, Luchini & Bottaro (2005). The disturbances are followed along their paths or rays by solving for the characteristics of the eikonal equation. The latter takes the form of the local dispersion relation of the Orr–Sommerfeld system. A review of complex-ray theory has been given by Chapman *et al.* (1999).

3.3. Optimal disturbances

We define optimal disturbances as those disturbances, $\mathbf{q} = (u, v, w, p)^T$, which will experience maximum energy amplification at a specific chordwise position x_1 for a given set of parameters Re, β, ω, x_0 . Because (3.8) poses an initial-value problem we are searching for the corresponding initial optimal disturbance $\mathbf{q}_0 = \mathbf{q}(x_0)$ which is introduced at the initial chordwise position x_0 .

3.3.1. Inner products

At this point it is useful to define those inner products which will be employed in the following. In order to measure the energy of a disturbance \mathbf{q} we define an energy norm

$$\|\mathbf{q}\|_E = (\mathbf{q}, M\mathbf{q}) \quad (3.12)$$

which is based on the inner product

$$(\Psi, \Phi) = \int_0^\infty \Psi^H \Phi \, dz \quad (3.13)$$

and $M = \text{diag}(1, 1, 1, 0)$ is necessary to assure that the pressure does not contribute; Ψ and Φ are \mathbf{C}_n -valued functions. Norm (3.12) represents a local measure of the disturbance energy at a specific location x . A global measure is given by

$$\langle \Psi, \Phi \rangle = \iint_{\Omega} \Psi^H \Phi \, dx \, dz, \quad (3.14)$$

where $\Omega = [x_0, x_1] \times [0, \infty]$ refers to the spatial domain. The adjoint of the differential operator L is then defined in terms of (3.14) as

$$\langle \mathbf{q}^*, L\mathbf{q} \rangle = \langle L^* \mathbf{q}^*, \mathbf{q} \rangle + \text{boundary terms}, \quad (3.15)$$

where $*$ denotes adjoint quantities and L^* represents the compact form of

$$L^* = \mathbf{A}^* + \mathbf{B}^* \frac{\partial}{\partial z} + \mathbf{C}^* \frac{\partial^2}{\partial z^2} + \mathbf{D}^* \frac{\partial}{\partial x}. \quad (3.16)$$

The derivation of the adjoint system as well as the specific forms of the adjoint operators \mathbf{A}^* , \mathbf{B}^* , \mathbf{C}^* and \mathbf{D}^* are presented in Appendix B.

3.3.2. Lagrange multipliers

The method of Lagrange multipliers will be used to set up the optimality system in the following. Our objective is to maximize the energy amplification at a specific chordwise position x_1 . A suitable objective function thus takes the form

$$J(\mathbf{q}) = \frac{\|\mathbf{q}_1\|_E}{\|\mathbf{q}_0\|_E}. \quad (3.17)$$

The subscripts 0 and 1 denote functions evaluated at the initial position x_0 and the position of maximum amplification x_1 respectively. Now we can define a Lagrange functional

$$\mathcal{L}(\mathbf{q}, \mathbf{q}^*) = J(\mathbf{q}) - \langle \mathbf{q}^*, \mathbf{L}\mathbf{q} \rangle, \quad (3.18)$$

where we have introduced a Lagrange multiplier or adjoint variable $\mathbf{q}^* = (p^*, u^*, v^*, w^*)^T$ enforcing the state variable to always satisfy the direct equations (3.8). In order to maximize the objective function (3.17) we need to find the stationary points of the Lagrange functional (3.18). These we get by finding the roots of the first variation of (3.18),

$$\delta \mathcal{L} = \langle \nabla_{\mathbf{q}^*} \mathcal{L}, \delta \mathbf{q}^* \rangle + \langle \nabla_{\mathbf{q}} \mathcal{L}, \delta \mathbf{q} \rangle = 0, \quad (3.19)$$

where $\nabla_{\mathbf{q}}$ denotes a gradient with respect to \mathbf{q} . For (3.19) to be fulfilled both inner products have to render zero independently. Considering the first inner product in (3.19) this implies solving the direct equations (3.8),

$$\langle \nabla_{\mathbf{q}^*} \mathcal{L}, \delta \mathbf{q}^* \rangle = 0 \Rightarrow \mathbf{L}\mathbf{q} = 0. \quad (3.20)$$

The first variation of (3.18) with respect to the state variable \mathbf{q} is most easily obtained by employing identity (3.15). Rendering the second inner product in (3.19) zero then implies

$$0 = \langle \nabla_{\mathbf{q}} \mathcal{L}, \delta \mathbf{q} \rangle \Leftrightarrow 0 = -\langle \mathbf{L}^* \mathbf{q}^*, \delta \mathbf{q} \rangle + \left(\mathbf{D}^H \mathbf{q}_0^* - 2 \frac{\|\mathbf{q}_1\|_E}{\|\mathbf{q}_0\|_E^2} M \mathbf{q}_0, \delta \mathbf{q}_0 \right) - \left(\mathbf{D}^H \mathbf{q}_1^* - \frac{2}{\|\mathbf{q}_0\|_E} M \mathbf{q}_1, \delta \mathbf{q}_1 \right), \quad (3.21)$$

if the boundary conditions for the adjoint variables are chosen such that the boundary terms of (3.15) vanish at $z = 0$ and $z \rightarrow \infty$. This is the case for

$$u^* = v^* = w^* = 0 \quad \text{at} \quad z = 0, \quad (3.22a)$$

$$u^* \rightarrow 0, v^* \rightarrow 0, w^* \rightarrow 0 \quad \text{as} \quad z \rightarrow \infty. \quad (3.22b)$$

In order for expression (3.21) to be true we require all inner products on the right-hand side to be zero independently for arbitrary $\delta \mathbf{q}$, $\delta \mathbf{q}_0$, $\delta \mathbf{q}_1$. Considering the first one retrieves the adjoint equations

$$\langle \mathbf{L}^* \mathbf{q}^*, \delta \mathbf{q} \rangle = 0 \Rightarrow \mathbf{L}^* \mathbf{q}^* = 0. \quad (3.23)$$

Optimality conditions are then provided by considering the second and the third inner product in (3.21). These can be interpreted as the first variations with respect to the initial disturbance and the disturbance at x_1 respectively. The corresponding

gradients of the Lagrange functional with respect to \mathbf{q}_0 and \mathbf{q}_1 take the form

$$\nabla_{\mathbf{q}_0} \mathcal{L} = \mathbf{D}^H \mathbf{q}_0^* - 2 \frac{\|\mathbf{q}_1\|_E}{\|\mathbf{q}_0\|_E^2} M \mathbf{q}_0, \quad (3.24)$$

$$\nabla_{\mathbf{q}_1} \mathcal{L} = -\mathbf{D}^H \mathbf{q}_1^* + \frac{2}{\|\mathbf{q}_0\|_E} M \mathbf{q}_1, \quad (3.25)$$

where the second term on the right-hand sides of both (3.24) and (3.25) arises from the objective function. The first term is a contribution of the boundary terms of (3.15), which after imposing boundary conditions (3.22) become $[(\mathbf{D}^H \mathbf{q}^*, \mathbf{q})]_{x_0}^{x_1}$ (see Appendix B).

At the stationary points of \mathcal{L} both gradients (3.24) and (3.25) are zero by definition. However, looking more closely at (3.24) and specifically at its first component,

$$\nabla_{u_0} \mathcal{L} = -2 \frac{\|\mathbf{q}_1\|_E}{\|\mathbf{q}_0\|_E^2} u_0 + U_0 u_0^* + p_0^*, \quad (3.26)$$

reveals that a zero gradient requires an initial disturbance component u_0 which is non-zero at the wall. This is because the adjoint equations (3.23) do not comprise a boundary condition for p^* , meaning that p_0^* is non-zero at the wall. Therefore, and because p^* proved to have a very small effect on the overall sensitivity with respect to \mathbf{q}_0 (see §4.3), we neglect it to assure that our optimal initial disturbance satisfies the boundary conditions. The optimality conditions thus take the form

$$u_0 = \frac{\|\mathbf{q}_0\|_E^2}{2\|\mathbf{q}_1\|_E} U_0 u_0^*, \quad (3.27a)$$

$$v_0 = \frac{\|\mathbf{q}_0\|_E^2}{2\|\mathbf{q}_1\|_E} U_0 v_0^*, \quad (3.27b)$$

$$w_0 = \frac{\|\mathbf{q}_0\|_E^2}{2\|\mathbf{q}_1\|_E} U_0 w_0^* \quad (3.27c)$$

at the initial chordwise position x_0 and

$$U_1 u_1^* + p_1^* = \frac{2}{\|\mathbf{q}_0\|} u_1, \quad (3.28a)$$

$$U_1 v_1^* = \frac{2}{\|\mathbf{q}_0\|} v_1, \quad (3.28b)$$

$$U_1 w_1^* = \frac{2}{\|\mathbf{q}_0\|} w_1 \quad (3.28c)$$

at the final chordwise position x_1 . Note that we do not obtain an optimality condition for p_0 because the weight matrix \mathbf{M} and the operator \mathbf{D}^H are singular, as their last rows consist of zeros. However, because we neglect the chordwise pressure gradient we do not need to prescribe the pressure at x_0 . By combining the continuity equation (3.6a) and the chordwise momentum equation (3.6b) p can be retrieved at each position according to

$$\begin{aligned} i\alpha p &= i\omega u - U_x u - U_z w + U i\beta v + U w_z - V i\beta u \\ &\quad - W u_z - \frac{1}{Re} (\alpha^2 u + \beta^2 u - u_{zz}). \end{aligned} \quad (3.29)$$

In the two-dimensional case, where $\alpha = 0$, the pressure term $i\alpha p$ becomes zero. The disturbance velocities are then directly related through (3.29). Therefore Andersson

et al. (1999) constrained the initial disturbance to satisfy (3.29) which leads to solving a least squares problem. However, in the three-dimensional case this becomes unnecessary, as the pressure term is non-zero. Hence, relation (3.29) is always fulfilled, and there is no need for a least squares solution for the initial disturbance.

The singularity of \mathbf{M} and \mathbf{D}^H also renders (3.28) overdetermined, leaving us to choose initial values for u_1^* and p_1^* arbitrarily as long as (3.28a) is satisfied. We simply set u_1^* to zero in the following. Any other choice would yield the same result though.

In order to obtain the optimal initial disturbance we need to solve the optimality system (3.20), (3.23), (3.27) and (3.28) which implies the following iterative procedure:

- (i) Choose an arbitrary initial disturbance $(u_0, v_0, w_0)^T$ satisfying (3.7).
- (ii) Solve the direct equations (3.20) marching from x_0 to x_1 .
- (iii) Obtain initial conditions for the adjoint equations according to (3.28) at x_1 .
- (iv) Solve the adjoint equations (3.23) by marching upstream from x_1 to x_0 .
- (v) Compute new candidate optimal initial disturbance according to (3.27) at x_0 .

Steps 2–5 are repeated until the growth is converged. Note that this approach does not guarantee a global maximum. It could just as well converge to a local extremum. However, starting from two different initial guesses this problem can be diminished.

3.4. Numerical approach

The numerical scheme to solve (3.8) is chosen similar to the one by Andersson *et al.* (1999). A second-order backward difference scheme is accomplished to discretize the direct equations in the chordwise direction, whereas the wall-normal direction is discretized employing a spectral collocation scheme based on Chebyshev polynomials. More details on the latter can be found in Hanifi *et al.* (1996). The same scheme is used to solve the adjoint equations (3.23) yielding the so-called discretized adjoint equations.

It should be noted that compared with the classical PSEs the approach outlined in §3.2 used here to solve (3.8) requires a higher resolution in the chordwise direction to yield a converged solution. To predict the modal amplification of crossflow modes a resolution roughly twice as high is required compared with the classical PSEs, which in turn results in about twice as much computation time. This is because the disturbance growth is completely captured by the amplitude functions \mathbf{q} . In order to yield the same accuracy and thus the same truncation error as for the classical PSEs, either the step size needs to be reduced, or the order of the scheme needs to be increased. For this reason, the classical PSE method is chosen in conjunction with the auxiliary function (3.5) to compute the evolution of modal disturbances in the following. Hence, if not stated explicitly, results on modal disturbances which are presented in §4 were obtained by employing the linear NOLOT code (see Hanifi *et al.* 1994) which represents an implementation of the classical PSE method.

4. Results

Solving the governing equations (3.8) by employing the approach described in §3.2 we are able to consider the general case of a non-parallel three-dimensional baseflow and to describe the spatial evolution of three-dimensional disturbances. We can therefore compute spatial optimal disturbances and give a measure for the potential initial amplification of crossflow modes because of non-modal growth.

The disturbance energy growth in a three-dimensional boundary layer constitutes a function

$$G = \frac{E_1}{E_0} = G(x_0, x_1, \beta, \omega, Re, \mathbf{q}_0). \quad (4.1)$$

The disturbance energy is denoted by $E = \|\mathbf{q}\|_E$. Obtaining the maximum growth for a given Reynolds number at a specific position x_1 thus implies finding the three optimal parameters x_0 , β and ω in addition to computing the shape function of the optimal initial disturbance \mathbf{q}_0 . If we want to know the maximum growth that is attainable along the chord of the flat plate the aforementioned optimal parameters and the optimal shape function need to be determined for several positions x_1 . This poses an expensive task in optimization which we are going to treat by combining the variational approach described in §3.3, which provides the optimal shape of the initial disturbance \mathbf{q}_0 with a Newton algorithm to find the optimal parameters x_0 , β and ω . However, before presenting results of such a ‘global’ optimization we will concentrate on the study of optimal growth of stationary disturbances. This is helpful in order to analyse the physical characteristics of optimal disturbances and to study the influence of individual parameters on optimal growth.

After validating our approach we study disturbance growth in FSC baseflows with a Reynolds number $Re_l = Q_\infty l/\nu = 10^6$. We consider three different sweep angles, namely $\Lambda = 25^\circ$, $\Lambda = 35^\circ$ and $\Lambda = 45^\circ$. The Hartree parameter is chosen to be either $\beta_H = 0.1$, yielding an accelerated boundary layer, or $\beta_H = -0.05$, which results in a decelerated boundary layer. Disturbance growth will in general be presented in form of N -factors,

$$N = 0.5 \log G, \quad (4.2)$$

or in form of the growth rate $\sigma = \partial N/\partial x$. If not specified explicitly all results presented throughout this section are scaled using the reference length $\delta = \sqrt{(l\nu/Q_l)}$ and the reference velocity Q_l , except for the chordwise coordinate x which is scaled with l .

4.1. Verification

In order to verify that the assumptions made in §3.1 (e.g. neglecting the chordwise disturbance pressure gradient p_x , capturing the disturbance growth in the shape functions) are appropriate a comparison with the DNS is presented in this section. The downstream evolution of a travelling and a stationary crossflow mode in an FSC boundary layer is computed by means of the here-developed modified PSEs and compared with the DNS results by Schrader *et al.* (2009) as well as the corresponding classical PSE solutions in figure 6. To conform to Schrader *et al.* (2009), non-dimensional values in figure 6 are based on the initial chordwise boundary layer displacement thickness and the initial chordwise free-stream velocity. All solutions match perfectly. The location of the neutral point as well as the disturbance growth are predicted similarly by all three approaches. Moreover, the real parts of the chordwise wavenumbers obtained from both PSE approaches match. Hence, the chordwise wavenumber which was determined iteratively on the basis of the lines of constant phase captures the major part of the periodic variation of \mathbf{q} as was assumed in §3.1. It should be noted that in order to obtain the good comparison with the DNS results also the classical PSE computations were performed without the p_x term. This was necessary in order to decrease the critical step size and to yield a sufficient resolution.

Further, the correct implementation of the adjoint equations (3.23) and the optimization procedure are verified in that the results reported by Levin &

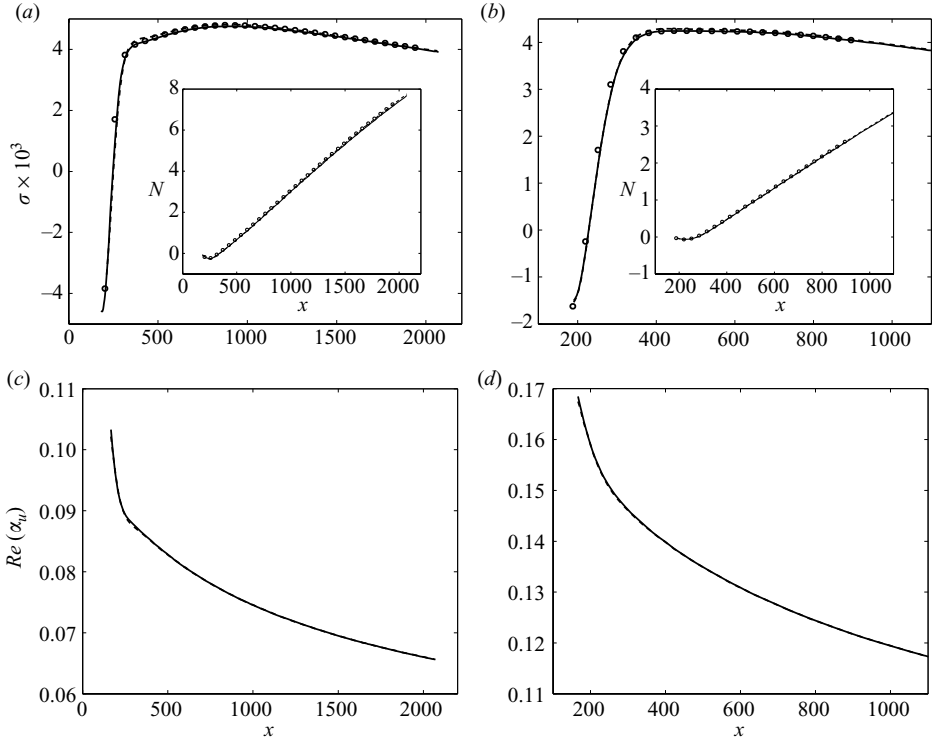


FIGURE 6. Evolution of crossflow modes in an FSC boundary layer studied by Schrader *et al.* (2009) with $\beta_H = 0.333$ and $\Lambda = 45^\circ$ computed by means of the here-developed modified PSEs (—), classical PSEs (---) and DNS (\circ). The growth rate σ , the N -factor and the real part of the chordwise wavenumber (only for the PSE methods) are shown for (a, c) a travelling crossflow mode with $\beta = -0.14$ and $\omega = -0.01$ and (b, d) a stationary crossflow mode with $\beta = -0.19$.

Henningson (2003) are reproduced for a Blasius boundary layer. The optimal growth $G = 0.0034Re_l$ at $x_1 = 1$ is obtained for $x_0 = 0.37$, $\beta = 0.53$ and $\omega = 0$. Considering a boundary layer with $\Lambda = 45^\circ$ and $\beta_H = 0$ which could also be seen as a swept Blasius boundary layer yields the same results and provides another check for our implementation of the chordwise wavenumber $\alpha = -\tan(\phi)\beta$ which was described in § 3.2.

4.2. Stationary disturbances

Although stationary disturbances proved to be optimal in two-dimensional boundary layers we cannot expect them to be optimal in the general three-dimensional case. However, stationary disturbances can play a major role in the transition process of three-dimensional boundary layers. This was found by Deyhle & Bippes (1996) who performed experimental investigations on disturbance growth in an unstable three-dimensional boundary layer. They found that stationary growth modes dominate in low-turbulence environments, whereas travelling modes become dominant in the presence of high levels of free-stream turbulence. From the point of view of transition it is thus also worthwhile to concentrate on optimal growth of stationary disturbances. Because we limit ourselves to the study of boundary layers with $Re_l = 10^6$ as mentioned above, the growth function to be investigated becomes $G = G(x_0, x_1, \beta, \mathbf{q}_0)$.

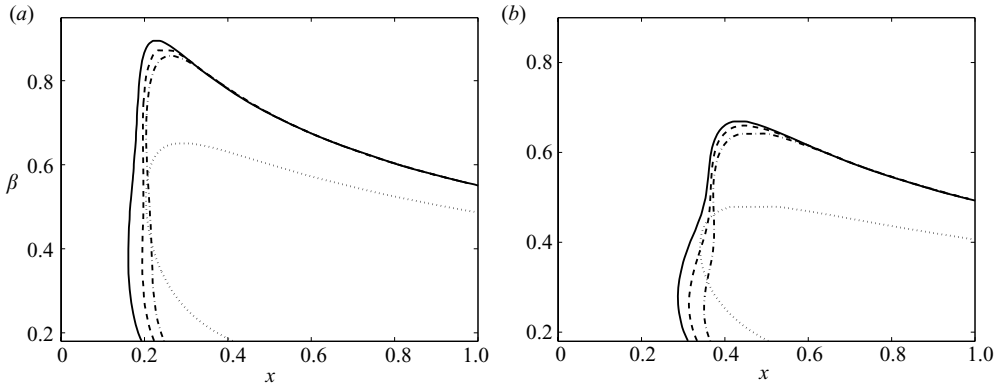


FIGURE 7. Neutral curves for stationary crossflow modes resulting from the classical PSE calculations for different initial positions x_0 and from solutions to the Orr–Sommerfeld equations. The neutral curves denote zero-disturbance energy growth. (a) An FSC boundary layer with $\beta_H = 0.1$ and $\Lambda = 45^\circ$. Neutral curves for $x_0 = 0.07$ (—), $x_0 = 0.1$ (---), $x_0 = 0.12$ (-·-), Orr–Sommerfeld solution (···). (b) An FSC boundary layer with $\beta_H = -0.05$ and $\Lambda = 45^\circ$. Neutral curves for $x_0 = 0.13$ (—), $x_0 = 0.15$ (---), $x_0 = 0.18$ (-·-), Orr–Sommerfeld solution (···).

4.2.1. Neutral curves for stationary modes

To be able to determine the extent of non-modal growth of a disturbance we need to know the location of the first neutral point of the corresponding modal instability. We get the latter by employing the classical PSE method. However, the neutral point of a modal instability predicted by PSEs is not well defined, as it depends on the position at which the initial disturbance is introduced. This is because the latter is usually chosen as a local solution to the Orr–Sommerfeld equations which comprise the parallel-flow assumption. Some transient effects which depend on the initial position and which effect the location of the neutral point will therefore be apparent initially. Figure 7 shows neutral curves of both the accelerated and the decelerated FSC boundary layer obtained from linear classical PSE calculations for three different initial positions. For comparison a neutral curve resulting from a local, parallel computation is also included. It is obvious that the position and the shape of the neutral curves vary for different initial positions. However, disregarding the local curve one can see that those parts of the curves that represent branch 2 fall on top of each other. The location of branch 1 moves upstream as the initial disturbance is introduced further upstream. The neutral curve corresponding to the local parallel computations is very different from those obtained by employing the PSEs. This indicates that non-local effects are important in this case.

For qualitative comparisons we choose the neutral curve yielding the largest supercritical domain in the following. The corresponding initial position x_0 is located as far upstream in the damped region as is possible to identify a discrete eigenmode. If quantitative comparisons are made both the modal and the optimal disturbance are introduced at the same position. Throughout the current paper we use the terms subcritical and supercritical to denote stable and unstable conditions with respect to the modal framework.

4.2.2. Optimal growth

As a first step we study optimal initial disturbances at a fixed initial position x_0 and compute the respective optimal growth that can be achieved at different positions x_1

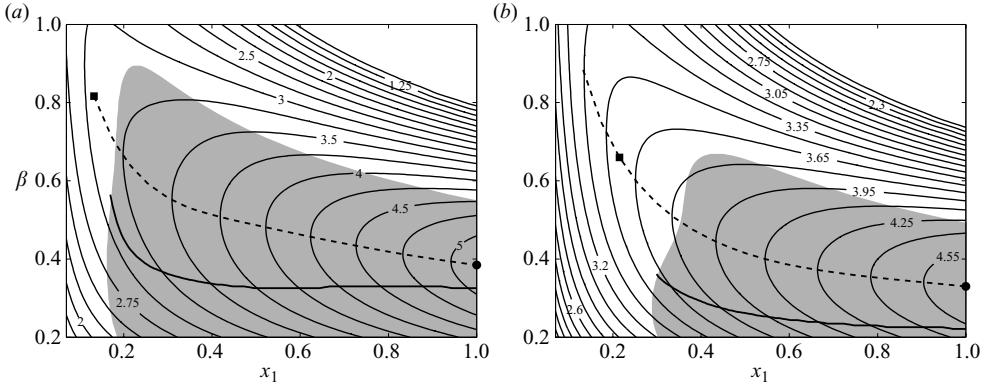


FIGURE 8. Contours of N -factors of \tilde{G} for steady disturbances and $x_0 = 0.01$. The dashed line denotes the optimal spanwise wavenumber β at each position x_1 obtained for optimal disturbances. The shaded region represents the largest supercritical domain of figure 7 and the solid line denotes the optimal β obtained from the corresponding classical PSE computations. (a) $\beta_H = 0.1$, $\Lambda = 45^\circ$, $\blacksquare \rightarrow (\beta = 0.82, x_1 = 0.13)$, $\bullet \rightarrow (\beta = 0.38, x_1 = 1)$. (b) $\beta_H = -0.05$, $\Lambda = 45^\circ$, $\blacksquare \rightarrow (\beta = 0.66, x_1 = 0.21)$, $\bullet \rightarrow (\beta = 0.33, x_1 = 1)$.

along the chord for different spanwise wavenumbers. In this case optimal growth is described by the function

$$\tilde{G} = \max_{q_0} G(x_1, \beta, \mathbf{q}_0). \quad (4.3)$$

Figure 8 shows \tilde{G} for an accelerated as well as a decelerated boundary layer, where the initial position was chosen as $x_0 = 0.01$ close to the leading edge. An important observation which can be made is that the disturbance growth is positive over almost the whole domain. Further, N -factors up to 3.5 in the accelerated boundary layer and up to 3.8 in the decelerated boundary layer are achieved even in the subcritical domains of the flow. A second observation can be made by considering the optimal spanwise wavenumber which yields maximum energy growth at each position x_1 . If we compare values of β yielding maximum growth of optimal disturbances with those yielding largest modal growth obtained from the classical PSE analysis we realize that these are quite different. For both boundary layers, the former takes relatively high values initially and decreases with increasing x_1 . For x_1 located well inside the supercritical domain it decreases almost linearly with increasing x_1 . The optimal spanwise wavenumber obtained from the linear classical PSE analysis on the other hand takes considerably smaller values which after decreasing initially become almost constant. This indicates that different crossflow modes are not equally susceptible to initial non-modal growth.

4.2.3. Optimal disturbances and the physical mechanisms of non-modal growth

In order to study the shape of optimal disturbances in the supercritical and subcritical domains of the flow we choose two positions for either of the two boundary layers that are considered in figure 8. A square symbol in figure 8 denotes subcritical parameters, whereas supercritical parameters are denoted by a circle. Comparing now the shape functions of the supercritical optimal disturbance with those of the subcritical one for the accelerated boundary layer reveals no principal differences as can be seen in figure 9. At the initial position the velocity components v_ϕ and w which are perpendicular to the line of constant phase dominate over u_ϕ . At the position of maximum amplification we observe a contrary situation in which the

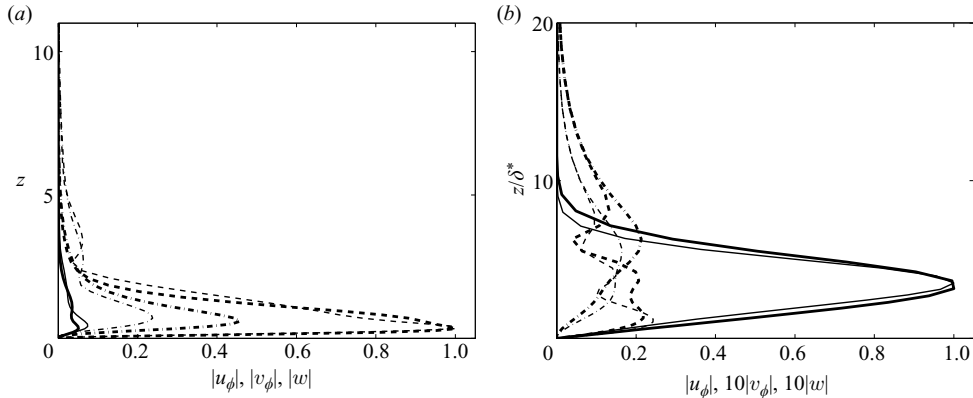


FIGURE 9. Shape functions of optimal disturbances for $\beta_H = 0.1$ and $\Lambda = 45^\circ$, where the velocities u_ϕ (—), v_ϕ (---) and w (-·-) are projected on to the x_ϕ , y_ϕ and z directions respectively. The thick lines correspond to the subcritical parameters denoted by the square in figure 8, and the thin lines correspond to the supercritical parameters denoted by the circle in figure 8. (a) Optimal initial condition. (b) Optimal disturbance at x_1 .

velocity component aligned with the line of constant phase becomes the dominating quantity, indicating a streak structure. The wall-normal position of the maximum streamwise velocity scales well with the local displacement thickness δ^* . Projecting the shape functions of the optimal disturbances on to a plane perpendicular to the lines of constant phase at both the initial and the final position the similarity between the subcritical and supercritical optimal disturbances becomes even more obvious (see figure 10). The projection reveals that optimal disturbances take the form of tilted vortices initially and evolve into bent streaks further downstream. The tilting directions in the accelerated and decelerated boundary layers are opposed. Projecting the shape functions on to the crossflow plane, as is done for the subcritical optimal disturbance in the accelerated boundary layer at three different chordwise positions in figure 11, reveals that the vortices are tilted against the mean shear of the crossflow initially. While travelling downstream they are erected within a very short distance. This process strongly resembles a two-dimensional non-modal growth mechanism discovered by Butler & Farrell (1992), which is based on the action of a perturbation Reynolds stress and is commonly referred to as the ‘Orr mechanism’. Åkervik *et al.* (2008) found this mechanism to provide the optimal way of initiating TS waves in the Blasius boundary layer. As opposed to the case of Couette flow considered by Butler & Farrell (1992), where the optimal disturbances are finally tilted in the direction of the mean crossflow shear they stay more or less upright in our case.

On the basis of the observations made so far we might thus conclude that the physical mechanism of non-modal growth in three-dimensional boundary layers is a combination of the well-known lift-up effect, where momentum is transferred to the streamwise component because of vortical motion, and the Orr mechanism.

Our observations confirm those of Corbett & Bottaro (2001) who found that in swept flows the algebraic growth mechanism and the exponential instability are complementary and excite disturbances of similar structure. The contrary can be found in two-dimensional boundary layers where these two mechanisms bear no resemblance. Employing a temporal framework Corbett & Bottaro (2001) found that the output state of an optimal disturbance for a slightly subcritical Reynolds number is very similar to the eigenfunction of the most amplified mode at a supercritical

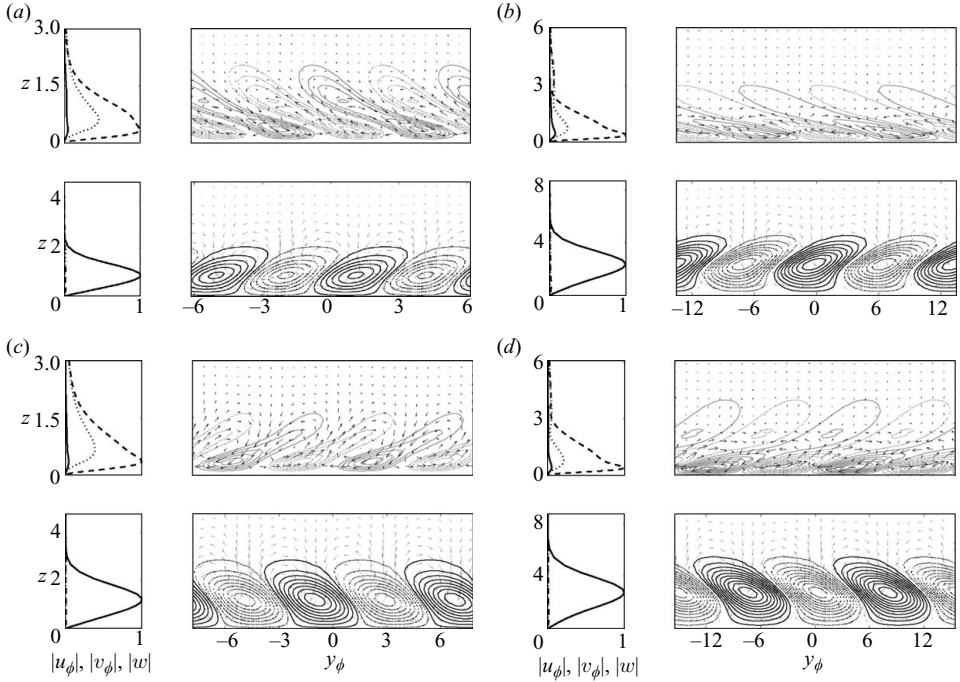


FIGURE 10. Optimal disturbances for $\Lambda = 45^\circ$. Each subplot corresponds to one of the four (β, x_1) -parameter pairs chosen in figure 8. Within each subplot, (left) absolute values of shape functions $|u_\phi|$, $|v_\phi|$ and $|w|$ and (right) projection of optimal disturbances on to a plane perpendicular to the lines of constant phase. The dominating quantities are denoted by black, while others are in grey. The contours denote the velocity components u_ϕ . The vectors represent v_ϕ and w respectively. Also shown are (upper) optimal initial disturbance at x_0 and (lower) downstream development of optimal disturbance at x_1 . (a) $\beta_H = 0.1$, subcritical parameters; (b) $\beta_H = 0.1$, supercritical parameters; (c) $\beta_H = -0.05$, subcritical parameters; (d) $\beta_H = -0.05$, supercritical parameters.

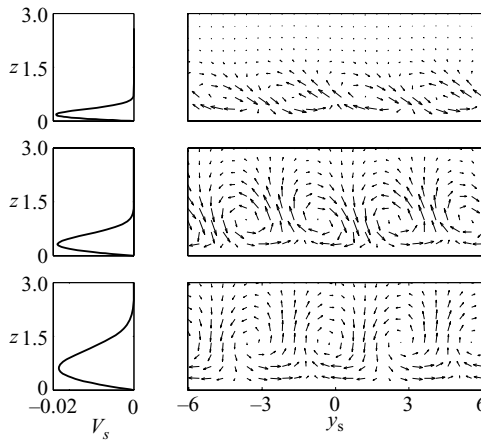


FIGURE 11. Visualization of Orr mechanism in an FSC boundary layer with $\Lambda = 45^\circ$ and $\beta_H = 0.1$; (β, x_1) correspond to the subcritical parameters chosen in figure 8. Shown on the right is the vector plot comprising the wall-normal and crossflow components of optimal disturbance at $x_0 = 0.01$ (upper), $x = 0.033$ (centre) and $x = 0.13$ (lower). Shown on the left are the mean crossflow components at the corresponding x positions.

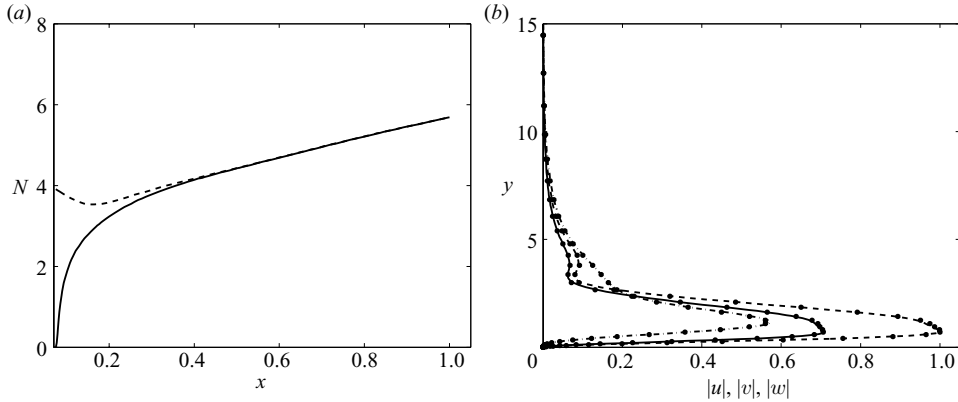


FIGURE 12. (a) The N -factors of optimal growth (—) and a pure crossflow mode (---) for $\omega = 0$, $\beta = 0.38$, $x_0 = 0.07$, $x_1 = 1$, $\Lambda = 45^\circ$ and $\beta_H = 0.1$. The curve representing the growth of the crossflow mode was shifted to match the optimal growth at $x = 1$. (b) The corresponding optimal initial disturbance (●) and shape functions of the adjoint crossflow mode at x_0 . The latter were multiplied with the chordwise velocity component of the meanflow $U(x_0)$, yielding u_0 (—), v_0 (---) and w_0 (-·-).

Reynolds number. On the basis of that observation they argued that algebraically growing disturbances are naturally fed into crossflow modes as the flow evolves. Employing our spatial approach we are able to observe this process. Figure 12 shows N -factors of a crossflow mode and the respective optimal disturbance whose spanwise wavenumbers correspond to the square in figure 8(a). The initial disturbances for both computations were introduced at the chordwise position $x_0 = 0.07$. Figure 12(a) depicts quite well how the optimal disturbance evolves into a discrete crossflow mode where the curve representing the growth of the crossflow mode is shifted to match the optimal growth curve in the last point. Some distance behind the neutral point of the crossflow mode both curves are identical. It thus becomes clear that crossflow modes adopt the role of optimal disturbances in supercritical regimes of the flow.

For such cases the adjoint optimal disturbance should resemble the adjoint of the corresponding crossflow mode (see Pralits *et al.* 2007). This means in turn that the optimal initial disturbance will be related to the adjoint crossflow mode through (3.27), yielding

$$\left. \begin{aligned} u_{opt}(x_0) &= cU(x_0)u_{CF}^*(x_0), \\ v_{opt}(x_0) &= cU(x_0)v_{CF}^*(x_0), \\ w_{opt}(x_0) &= cU(x_0)w_{CF}^*(x_0), \end{aligned} \right\} \quad (4.4)$$

where c represents a scaling factor and the subscript CF denotes quantities of a dominating crossflow mode. Figure 12(b) shows such a comparison between an optimal initial disturbance which maximizes the energy growth at $x = 1$ and the corresponding adjoint crossflow mode at x_0 which is modified according to (4.4). Both sets of shape functions match perfectly. The adjoint crossflow mode is computed using an adjoint PSE solver based on the NOLOT code mentioned earlier (see Pralits *et al.* 2000).

4.2.4. Optimal initial amplification of modal disturbances

The last section exemplified how optimal disturbances develop into crossflow modes. We now want to determine the equivalent initial energy that the pure discrete

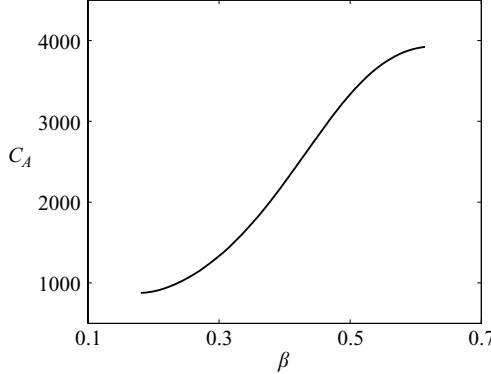


FIGURE 13. Optimal initial energy of stationary crossflow modes in an FSC boundary layer with $\Lambda = 45^\circ$ and $\beta_H = 0.1$. All disturbances were introduced at $x_0 = 0.07$, and the position of maximum amplification is $x_1 = 1$.

eigenmode should have such that its energy matches the growth, or in other words the normalized energy, of the optimal disturbance at x_1 . This ‘optimal initial energy’ tells us how susceptible the excited crossflow mode is to initial non-modal growth. It is obtained by introducing both the optimal initial disturbance and the corresponding local eigenmode at the same position. The growth curve of the pure crossflow mode is then shifted such that it matches the optimal growth curve in the last point as presented in figure 12(a). A corresponding amplification coefficient may be defined as

$$C_A = \frac{E_{0,CF}}{E_{0,opt}}, \quad (4.5)$$

where $E_{0,opt}$ denotes the energy of the optimal initial disturbance and $E_{0,CF}$ denotes the optimal initial energy of the pure excited crossflow mode, which was determined as described above. It should be noted that the natural logarithm of C_A is related to the amplification factor defined in Pralits *et al.* (2007).

If we calculate C_A for several modes with $\beta = 0.18$ – 0.61 we obtain the curve presented in figure 13. It becomes clear that C_A increases with β for the range of wavenumbers considered here. This shows that the potential for initial amplification of different crossflow modes because of non-modal growth is diverse. We have already found an indication for this by comparing the optimal spanwise wavenumbers of crossflow modes and optimal disturbances in figure 8.

4.2.5. Dependence of optimal growth on initial position x_0

Levin & Henningson (2003) found the optimal initial position in a Blasius boundary layer to be $x_0 = 0.37$, a considerable distance downstream of the leading edge. So far we have only considered fixed initial positions x_0 at which the disturbances were introduced into the boundary layer. We now investigate the influence of x_0 on optimal growth in FSC boundary layers. Therefore we fix the position of maximum amplification to be $x_1 = 1$. Hence, optimal growth is computed according to

$$\tilde{G} = \max_{q_0} G(x_0, \beta, q_0); \quad (4.6)$$

\tilde{G} is presented in figure 14 for the accelerated as well as the decelerated FSC boundary layer. It becomes apparent that similar to the two-dimensional case, the optimal initial position which depends on the spanwise wavenumber is located a

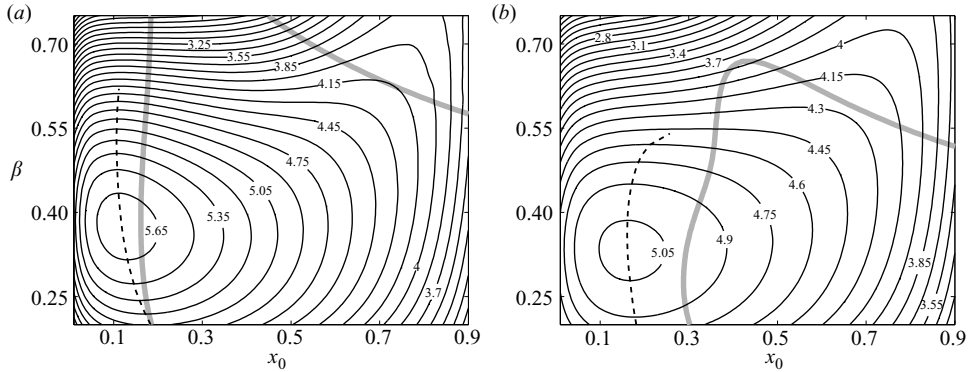


FIGURE 14. Contours of optimal growth of stationary disturbances at $x_1 = 1$. The dashed line denotes the optimal initial position for those optimal disturbances experiencing exponential growth at $x_1 = 1$. The thick grey line corresponds to the neutral curves of stationary crossflow modes and represents the most unstable case shown in figure 7(a, b). (a) $\beta_H = 0.1$, $\Lambda = 45^\circ$. (b) $\beta_H = -0.05$, $\Lambda = 45^\circ$.

certain distance downstream of the leading edge. The dashed, almost-vertical lines in figure 14 denote the optimal initial position for those optimal disturbances that experience exponential growth at $x_1 = 1$. The position of these lines does not exactly correspond to the position of branch 1 in either case. However, keeping in mind that the position of branch 1 depends on the initial position and that it moves upstream if the disturbances are introduced further upstream one could, at least in the accelerated case, argue that the optimal initial position is located around the region of neutral stability.

For disturbances with $\beta > 0.6$ in the accelerated and $\beta > 0.55$ in the decelerated boundary layer, the optimal initial position moves close to x_1 . The reason for this phenomenon is found in the eventual decay of disturbances. At $x_1 = 1$ these spanwise wavenumbers denote a subcritical region in terms of exponential growth. Hence, if the corresponding disturbances are introduced far upstream of the final position x_1 they will experience non-modal growth initially but will eventually decay further downstream. However, if the disturbances are introduced close enough, non-modal growth is still present close to or at the position of maximum amplification. Thus, optimal growth for such subcritical parameters is obtained for initial positions which are located close to x_1 .

4.2.6. Dependence of optimal growth on the sweep angle

In this section we study optimal growth of steady disturbances in both accelerated and decelerated FSC boundary layers with three different sweep angles, namely $\Lambda = 45^\circ$, $\Lambda = 35^\circ$ and $\Lambda = 25^\circ$. The optimal growth function which is investigated now becomes

$$\tilde{G} = \max_{q_0} G(\Lambda, \beta, q_0). \quad (4.7)$$

We start by comparing the optimal non-modal growth at a position x_1 which denotes subcritical conditions in all six different boundary layers. Therefore x_1 is chosen to be located upstream of the first neutral point of the accelerated boundary layer with $\Lambda = 45^\circ$ which represents the most unstable one. Hence, $x_1 = 0.13$ which corresponds to the square symbol in figure 8(a) is a suitable choice. Figure 15 presents the optimal non-modal growth obtained for different spanwise wavenumbers for all boundary

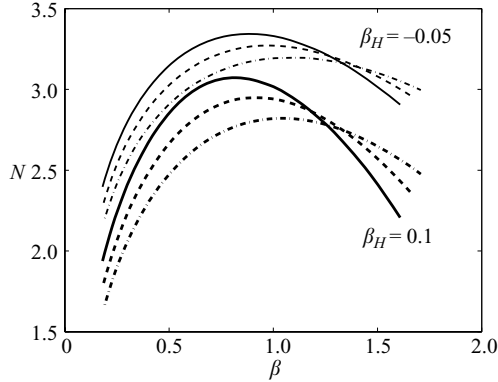


FIGURE 15. The N -factors of optimal growth at $x_1 = 0.13$ (subcritical) for $x_0 = 0.01$, $\omega = 0$, $\beta_H = 0.1$ (thick lines) and $\beta_H = -0.05$ (thin lines). FSC boundary layers with different sweep angles $\Lambda = 45^\circ$ (—), $\Lambda = 35^\circ$ (---), $\Lambda = 25^\circ$ (-.-) are considered.

layers. It is noticeable that all three decelerated boundary layers exhibit larger N -factors of optimal non-modal growth than the accelerated ones. This result is in accordance with the findings by Corbett & Bottaro (2000) and Levin & Henningson (2003) for two-dimensional boundary layers and Corbett & Bottaro (2001) for three-dimensional boundary layers, who observed higher levels of non-modal growth for adverse pressure gradients. Further we find that the maximum growth achievable at x_1 increases for increasing sweep angles. Hence, the larger the crossflow in a boundary layer the larger the maximum non-modal growth. Considering the six boundary layers at hand the overall maximum growth is obtained for $\beta_H = -0.05$ and $\Lambda = 45^\circ$.

We observe a similar picture if we examine the optimal growth in the supercritical domains of three accelerated boundary layers with different sweep angles as shown in figure 16(a). Because the corresponding optimal disturbances eventually evolve into crossflow modes it is interesting to compute the optimal initial amplification C_A of the crossflow modes as done in §4.2.2. To do so, both the optimal initial disturbance and the discrete eigenmode need to be introduced at the same position x_0 . The position furthest upstream at which we could find a discrete eigenmode for all three boundary layers is $x_0 = 0.16$. Further, C_A is presented in figure 16(c). It is noteworthy that although maximum growth is obtained for the largest sweep angle and thus for the boundary layer with the largest crossflow, maximum initial amplification of crossflow modes is obtained for $\Lambda = 25^\circ$. On the basis of this result one might conclude that non-modal growth becomes more relevant for boundary layers with small sweep angles. This seems logical as exponential growth sets in earlier for larger sweep angles, resulting in a smaller region of non-modal growth. Hence, the disturbance growth at the point of neutral stability decreases for increasing sweep angles. The disparity regarding initial amplification of crossflow modes obtained for the two different initial positions in figures 13 and 16 for $\Lambda = 45^\circ$ is related to the results in §4.2.5 and shows that x_0 has an influence on optimal initial amplification of discrete modes.

4.3. Global optimal disturbances

The term ‘global’ is used in the sense that we optimize the disturbance growth not only with respect to the initial shape function but also regarding the spanwise wavenumber, the frequency and the initial position at which disturbances are introduced. The

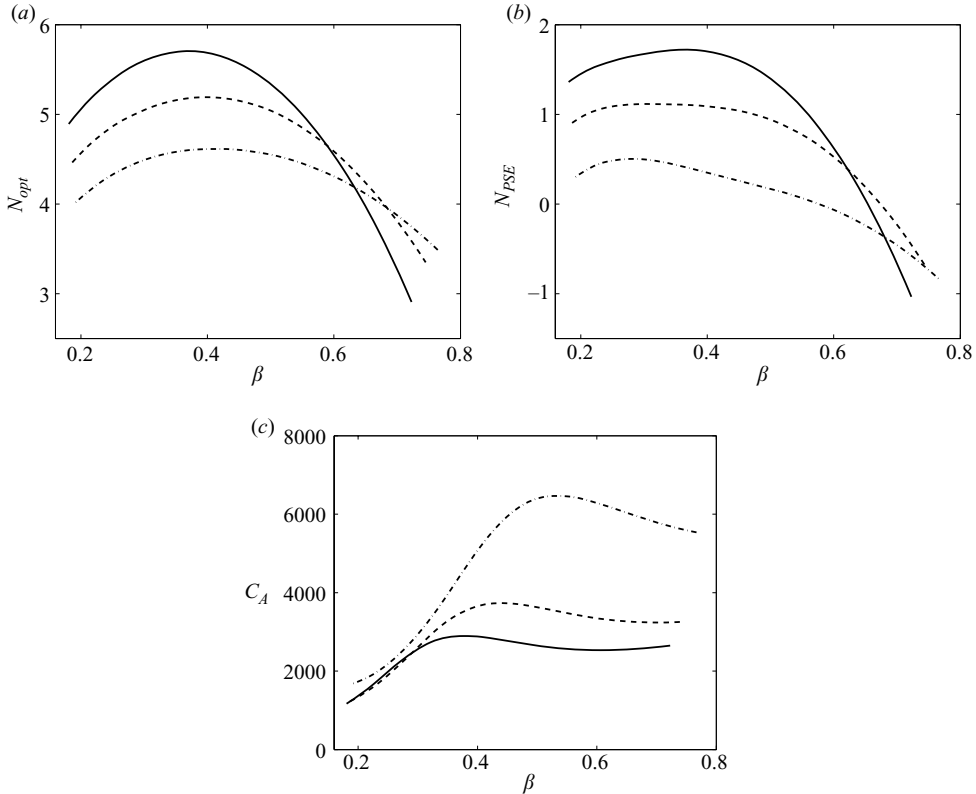


FIGURE 16. (a) The N -factors of optimal growth at $x_1 = 1$ for $x_0 = 0.16$, $\omega = 0$, $\beta_H = 0.1$ and three different sweep angles, namely $\Lambda = 45^\circ$ (—), $\Lambda = 35^\circ$ (---), $\Lambda = 25^\circ$ (-.-). (b) The N -factors of crossflow modes for the same parameters as in (a), calculated using the classical PSE. (c) Optimal initial amplification of crossflow modes at $x_0 = 0.16$.

respective function describing global optimal growth is thus defined as

$$\bar{G} = \max_{x_0, \beta, \omega, \mathbf{q}_0} G(x_0, x_1, \beta, \omega, \mathbf{q}_0). \quad (4.8)$$

Obtaining \bar{G} involves a more complex optimization procedure. In addition to employing the adjoint-based optimization procedure described in § 3.3, which provides the optimal initial disturbance shape, we now also need to determine x_0 , β , ω , yielding the maximum possible disturbance growth at each x_1 . These we get by utilizing Newton's line search method in which each iteration step is given according to

$$\begin{pmatrix} x_0 \\ \beta \\ \omega \end{pmatrix}_{k+1} = \begin{pmatrix} x_0 \\ \beta \\ \omega \end{pmatrix}_k - \gamma_k \nabla^2 \tilde{G}, \quad (4.9)$$

with

$$\tilde{G} = \max_{\mathbf{q}_0} G(x_0, x_1, \beta, \omega, \mathbf{q}_0). \quad (4.10)$$

The largest step length γ which yields an increase in \tilde{G} is provided via backtracking. The Hessian matrix $\nabla^2 \tilde{G}$ is computed using finite differences. We thus need to perform 10 evaluations of \tilde{G} for each Newton step. Iterations are performed until the norm

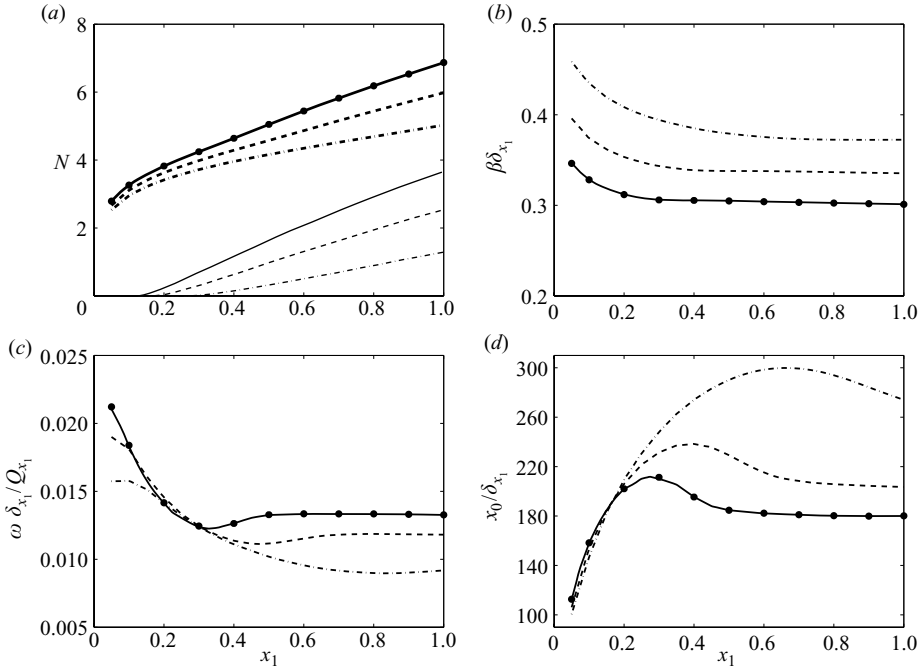


FIGURE 17. The thick lines represents N -factors and the corresponding optimal parameters for global optimal growth. The thin lines in (a) represent N -factors from a solution to the classical PSE. Also shown are the results for $\beta_H = 0.1$ and sweep angles $\Lambda = 45^\circ$ (—), $\Lambda = 35^\circ$ (---), $\Lambda = 25^\circ$ (-.-); ● represents calculations with the unphysical optimality condition (see § 3.3). The parameters (β, ω, x_0) are non-dimensionalized with the local reference values δ_{x_1} and Q_{x_1} . The plots show (a) N -factors, (b) optimal spanwise wavenumber, (c) optimal frequency and (d) optimal initial position.

of the gradient is less than $\|\nabla \tilde{G}_k\|_2 / \tilde{G}_k < 10^{-3}$ which for all performed calculations corresponded to a relative change $\Delta \tilde{G} = |\tilde{G}_{k+1} - \tilde{G}_k| / \tilde{G}_k = O(10^{-6})$ or less.

We once more use the Blasius boundary layer to verify this approach. The maximum growth $\bar{G} = 0.0034 Re_{x_1}$ is obtained for the optimal parameters $\beta = 0.53$, $\omega = 0$ and $x_0 = 0.375$ and thus reproduces the results by Levin & Henningson (2003). In order to obtain an envelope comprising non-modal growth we compute \bar{G} for several positions x_1 along the chord of the plate. We consider the six FSC boundary layers which exhibit different pressure gradients and sweep angles and were already examined in the latter section § 4.2.6.

4.3.1. Accelerated boundary layers

Figure 17 depicts results of the global optimization approach for three accelerated boundary layers with $\beta_H = 0.1$ and sweep angles $\Lambda = 45^\circ$, $\Lambda = 35^\circ$ and $\Lambda = 25^\circ$. Figure 17(a) compares global optimal growth with envelopes which are based on modal growth solely. The latter are obtained from a classical parametric PSE study. It clearly shows that the maximum growth which can be achieved by introducing optimal initial disturbances with optimal parameters β , ω and x_0 into the boundary layers can be two to three orders of magnitude larger compared with what is predicted on the basis of modal analysis. Substantial disturbance growth is obtained at all stations. Even at subcritical conditions close to the leading edge N -factors between two and three are possible. Such a large and rapid disturbance growth

could lead to early nonlinear effects. It is noticeable that the optimal parameters β , ω and x_0 scale with the local reference values $\delta_{x_1} = \sqrt{\nu x_1 / Q_{x_1}}$ and $Q_{x_1} = Q_e(x_1)$ once x_1 is located well inside the supercritical region of the boundary layer as can be seen in figure 17(b–d). The superscript e denotes the boundary layer edge. The corresponding dimensional optimal spanwise wavenumber and frequency decrease with x_1 , whereas the dimensional optimal initial position increases. Figure 17(c) reveals another difference with respect to two-dimensional boundary layers as the optimal frequency is non-zero. For a Blasius boundary layer Luchini (2000) showed that $\omega = 0$ represents the optimal frequency.

All optimization results presented so far were computed using the optimality conditions (3.27). However, we described in §3.3 that these had to be modified, as $p^*(x_0)$ was neglected to yield an optimal initial disturbance satisfying no-slip conditions at the wall. To study the effect of this modification on optimal growth we compute the global optimal growth for a limited number of positions x_1 using the unphysical optimality condition (3.26) and compare it with the results that we obtained using the modified optimality condition. Figure 17 shows that the results from both computations are identical. The reason is that $p^*(x_0)$ is found to be of considerable size only close to the wall. Because the initial non-zero value at the boundary is forced to zero immediately when integrating downstream, the effect of $p^*(x_0)$ is insignificant. Our assumption that the modification does not influence the optimization is therefore justified.

4.3.2. Decelerated boundary layers

Performing the global optimization for decelerated boundary layers using the above-described method is not as straightforward as for their accelerated counterparts. The reason is the occurrence of TS waves. In adverse pressure gradient boundary layers these can become strongly amplified and dominate over crossflow modes. TS waves will thus adopt the role of optimal disturbances at some distance from the leading edge. Yet our method is not designed to describe the spatial evolution of TS waves. The reason is our approach to determine lines of constant phase. Our assumption that these closely follow the outer streamline and that u_ϕ represents the dominating flow quantity of the flow is no longer true for TS waves. Their lines of constant phase are usually close to being perpendicular with respect to the outer streamline. Initiating the iteration procedure with the external streamline as described in §3.2 thus constitutes the worst case regarding a TS wave and does not yield a converged solution. We will therefore be able to compute global optimal disturbances in decelerated boundary layers up to the point at which TS waves become the optimal disturbances.

On applying the global optimization method to an FSC boundary layer with $\beta_H = -0.05$ and $\Lambda = 45^\circ$, the situation illustrated in figure 18 is observed. The Newton iterations converge until $x_1 = 0.375$. For chordwise positions larger than that the Newton method tends to considerably lower spanwise wavenumbers for which the adjoint-based optimization does not converge. Figure 18 depicts a rather qualitative comparison between optimal growth and modal growth of the most amplified TS waves which were all initiated close to their neutral point. It is obvious though that around $x_1 = 0.375$ optimal growth and modal growth of TS waves are of the same order of magnitude. The occurrence of TS waves becoming the most amplified disturbance constitutes the most natural explanation. However, the global optimization procedure works well for $x_1 < 0.375$. This region is of great interest because rapid and extensive initial disturbance growth can lead to early nonlinear effects which in turn can lead to the formation of secondary instabilities

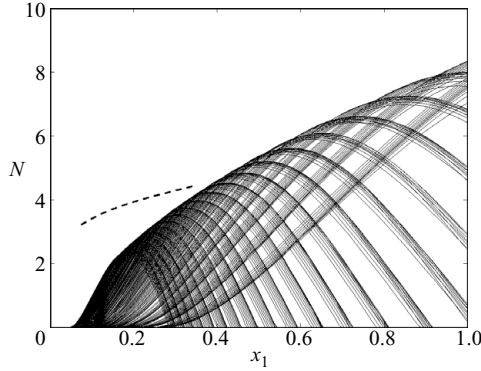


FIGURE 18. The N -factors of global optimal growth (---) and TS waves (—) for a decelerated FSC boundary layer with $\beta_H = -0.05$ and $\Lambda = 45^\circ$.

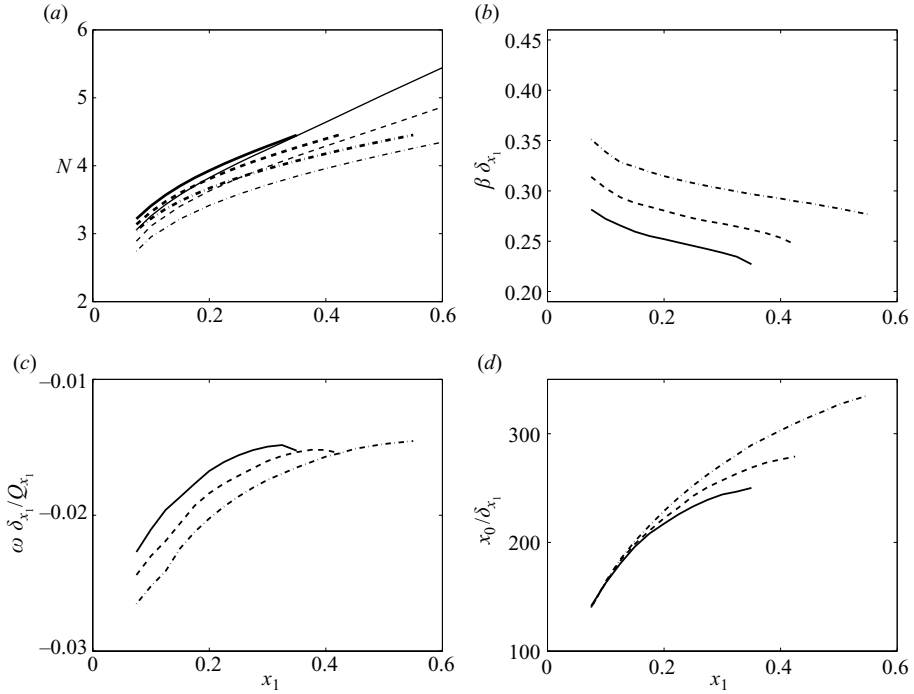


FIGURE 19. The N -factors and corresponding optimal parameters for global optimal growth for baseflows with $\beta_H = -0.05$ and sweep angles $\Lambda = 45^\circ$ (—), $\Lambda = 35^\circ$ (---), $\Lambda = 25^\circ$ (-.-). the thin lines in (a) represent the N -factors of global optimal growth for respective baseflows with $\beta_H = 0.1$. The parameters (β, ω, x_0) are non-dimensionalized with the local reference values δ_{x_1} and Q_{x_1} . The plots are as follows (a) N -factors, (b) optimal spanwise wavenumber, (c) optimal frequency and (d) optimal initial position.

and a breakdown to turbulence. The following optimization results for decelerated boundary layers are therefore presented for those regions in which TS waves do not dominate.

Figure 19 shows the global optimal growth together with the corresponding optimal parameters which were obtained for three decelerated boundary layers with different

sweep angles. Figure 19(a) compares the global optimal growth in the front part of the flat plate with the maximum possible growth found in the accelerated boundary layers. The comparison shows that the maximum non-modal growth in decelerated boundary layers is larger and thus corresponds to the results found for stationary disturbances presented in figure 15. Hence, decelerated boundary layers also have a potential for strong and rapid disturbance growth already very close to the leading edge. As for the accelerated boundary layer it is therefore important to take into account non-modal growth when trying to predict the transition location. The optimal values for β , ω and x_0 presented in figure 19(b–d) do not scale with the local reference values in the range that could be considered here. The corresponding dimensional values of the spanwise wavenumber decrease with x_1 where those of the frequency and the initial position increase. As was found for accelerated boundary layers, the optimal frequency is non-zero for decelerated three-dimensional boundary layers.

5. Conclusions

Optimal growth has been studied in accelerated as well as decelerated FSC boundary layers at different sweep angles. To be able to perform a numerically efficient parametric study a parabolized set of equations was developed, allowing for the description of both modal and non-modal linear growth of disturbances whose lines of constant phase are closely aligned with the external streamline. For reasons related to the need to capture all the disturbance growth in the shape function, strongly growing disturbances may fall outside the scope of application though. The Lagrange multiplier technique was employed to derive an optimality system, yielding optimal initial disturbances. The governing equations and our approach to solve them have been verified by comparing the predicted spatial evolution of crossflow modes with the DNS results by Schrader *et al.* (2009) and the corresponding result of a classical PSE method. In addition, results for optimal growth in a Blasius boundary layer were reproduced correctly, verifying our optimization procedure.

Considering the results obtained for stationary disturbances it becomes clear that no principle difference exists regarding optimal disturbances at subcritical and supercritical conditions in three-dimensional boundary layers. Optimal disturbances take the form of streamwise-oriented vortices which are tilted against the mean shear of the crossflow initially and evolve into bent streaks further downstream, which are almost aligned with the external streamline. When entering the supercritical domain of the boundary layer, optimal disturbances smoothly evolve into the dominating eigenmodes. The initially tilted vortical structures quickly rise into an upright position while moving downstream. On the basis of these observations we have argued that the physical mechanism driving non-modal growth in three-dimensional boundary layers consists of a combination of the lift-up effect and the Orr mechanism.

The fact that optimal disturbances at both subcritical and supercritical conditions share the same characteristics is in contrast with two-dimensional boundary layers where streaks and TS waves bear no resemblance and confirms the findings by Corbett & Bottaro (2001). It is therefore concluded that non-modal growth initiates modal instabilities in form of crossflow modes in three-dimensional boundary layers. Computing the optimal initial amplification of different modes showed that these are not equally susceptible to non-modal growth. This important effect is not taken care of by classical transition prediction methods such as the e^N method, which solely consider modal growth.

The position at which disturbances should be introduced to optimally excite stationary crossflow modes in an accelerated boundary layer was found to be located around the region of neutral stability. Such a relation is not as clear in the decelerated boundary layer considered, where the optimal initial position is located upstream of the neutral point.

It was found that maximum non-modal growth at subcritical conditions is larger for adverse pressure gradients, complying again with the results by Corbett & Bottaro (2001), and that it increases for increasing sweep angles. However, computing the optimal initial energy of modal instabilities for boundary layers of different sweep angles revealed that non-modal growth becomes more relevant for smaller sweep angles. Hence, the smaller the sweep angle, the larger the initial amplification of modal instabilities.

Finally, we computed global optimal growth for non-stationary disturbances. The term global refers to optimization with respect to the spanwise wavenumber, frequency and initial position in addition to optimization with respect to the initial disturbance shape. This was achieved by combining adjoint-based optimization, yielding the optimal shape function with a Newton line search algorithm providing the three above-mentioned optimal parameters β , ω and x_0 . Global optimal growth was computed for several positions on the plate where both accelerated and decelerated boundary layers with several sweep angles were considered. In general disturbance growth was found at all positions on the flat plate where the global optimal disturbances are non-stationary as opposed to the case of two-dimensional boundary layers. The considered accelerated boundary layers exhibited disturbance growth $O(10^2)$ – $O(10^3)$ already at subcritical conditions. At supercritical conditions the computed global optimal growth exceeded the maximum predicted modal growth by two to three orders of magnitude.

In decelerated boundary layers global optimal growth could only be computed up to the position at which TS waves become dominant because the herein-developed method cannot predict the evolution of TS waves. However it was shown that up to that position disturbance growth $O(10)$ – $O(10^4)$ is possible if non-modal growth is considered.

These results show that non-modal growth is of considerable size in three-dimensional boundary layers and could therefore lead to early nonlinear effects. As both free-stream turbulence and wall roughness are likely to cause disturbances similar in shape to the here-obtained optimal disturbances non-modal growth may be related to a receptivity mechanism for modal instabilities and should therefore not be disregarded when determining the location at which transition from laminar to turbulent flow occurs. Future work will therefore determine how optimal growth can be associated with receptivity coefficients, describing the initial amplification of crossflow modes because of e.g. free-stream turbulence.

The authors would like to thank Luca Brandt, Lars-Uve Schrader, Antonios Monokrousos and Yohann Duguet for fruitful discussions. This work is supported by the European Commission through the FP6 project ‘TELFONA’ (contract no. AST4-CT-2005-516109).

Appendix A. Operators of the direct equations

In §3.1 the set of parabolic equations (3.6) is expressed in operator form as

$$Lq = 0 \tag{A 1}$$

with \mathbf{L} being a linear operator of the form

$$\mathbf{L} = \mathbf{A} + \mathbf{B} \frac{\partial}{\partial z} + \mathbf{C} \frac{\partial^2}{\partial z^2} + \mathbf{D} \frac{\partial}{\partial x} \quad (\text{A } 2)$$

and $\mathbf{q} = (u, v, w, p)^T$ representing the state vector. The individual linear operators \mathbf{A} , \mathbf{B} , \mathbf{C} and \mathbf{D} take the form

$$\mathbf{A} = \begin{pmatrix} i\alpha & i\beta & 0 & 0 \\ C + U_x & 0 & U_z & i\alpha \\ V_x & C & V_z & i\beta \\ 0 & 0 & C + W_z & 0 \end{pmatrix}, \quad (\text{A } 3)$$

$$\mathbf{B} = \begin{pmatrix} 0 & 0 & 1 & 0 \\ W & 0 & 0 & 0 \\ 0 & W & 0 & 0 \\ 0 & 0 & W & 1 \end{pmatrix}, \quad (\text{A } 4)$$

$$\mathbf{C} = \begin{pmatrix} 0 & 0 & 0 & 0 \\ -\frac{1}{Re} & 0 & 0 & 0 \\ 0 & -\frac{1}{Re} & 0 & 0 \\ 0 & 0 & -\frac{1}{Re} & 0 \end{pmatrix}, \quad (\text{A } 5)$$

$$\mathbf{D} = \begin{pmatrix} 1 & 0 & 0 & 0 \\ U & 0 & 0 & 0 \\ 0 & U & 0 & 0 \\ 0 & 0 & U & 0 \end{pmatrix}, \quad (\text{A } 6)$$

where

$$C = -i\omega + i\alpha U + i\beta V + \frac{1}{Re}(\alpha^2 + \beta^2). \quad (\text{A } 7)$$

Appendix B. Derivation of the adjoint operators

In §3.3.1 the adjoint of the direct operator \mathbf{L} is defined in terms of the inner product (3.14) as

$$\langle \mathbf{q}^*, \mathbf{L}\mathbf{q} \rangle = \langle \mathbf{L}^* \mathbf{q}^*, \mathbf{q} \rangle + \text{boundary terms}, \quad (\text{B } 1)$$

where $*$ denotes adjoint quantities and \mathbf{L}^* represents the compact form of

$$\mathbf{L}^* = \mathbf{A}^* + \mathbf{B}^* \frac{\partial}{\partial z} + \mathbf{C}^* \frac{\partial^2}{\partial z^2} + \mathbf{D}^* \frac{\partial}{\partial x}. \quad (\text{B } 2)$$

In order to obtain the specific forms of the adjoint operators \mathbf{A}^* , \mathbf{B}^* , \mathbf{C}^* and \mathbf{D}^* we need to perform integration by parts on the leftmost inner product in (B 1), yielding

$$\begin{aligned} & \int \int_{\Omega} (\mathbf{q}^*)^H \left(\mathbf{A}\mathbf{q} + \mathbf{B} \frac{\partial \mathbf{q}}{\partial z} + \mathbf{C} \frac{\partial^2 \mathbf{q}}{\partial z^2} + \mathbf{D} \frac{\partial \mathbf{q}}{\partial x} \right) dx dz \\ &= \int \int_{\Omega} \left(\mathbf{A}^* \mathbf{q}^* + \mathbf{B}^* \frac{\partial \mathbf{q}^*}{\partial z} + \mathbf{C}^* \frac{\partial^2 \mathbf{q}^*}{\partial z^2} + \mathbf{D}^* \frac{\partial \mathbf{q}^*}{\partial x} \right)^H \mathbf{q} dx dz \\ &+ \int_{x_0}^{x_1} \left[(\mathbf{q}^*)^H \left(\mathbf{B}\mathbf{q} + \mathbf{C} \frac{\partial \mathbf{q}}{\partial z} - \frac{\partial \mathbf{C}}{\partial z} \mathbf{q} \right) - \left(\frac{\partial \mathbf{q}^*}{\partial z} \right)^H \mathbf{C}\mathbf{q} \right]_{z=0}^{z=\infty} dx \\ &+ \int_0^{\infty} [(\mathbf{q}^*)^H \mathbf{D}\mathbf{q}]_{x_0}^{x_1} dz \end{aligned} \quad (\text{B } 3)$$

with

$$\mathbf{A}^* = \mathbf{A}^H - \frac{\partial \mathbf{B}^H}{\partial z} + \frac{\partial^2 \mathbf{C}^H}{\partial z^2} - \frac{\partial \mathbf{D}^H}{\partial x}, \quad (\text{B } 4)$$

$$\mathbf{B}^* = -\mathbf{B}^H + 2 \frac{\partial \mathbf{C}^H}{\partial z}, \quad (\text{B } 5)$$

$$\mathbf{C}^* = \mathbf{C}^H, \quad (\text{B } 6)$$

$$\mathbf{D}^* = -\mathbf{D}^H. \quad (\text{B } 7)$$

The boundary terms at $z = 0$ and $z = \infty$ in (B3) become zero if the boundary conditions for the adjoint variables u^* , v^* and w^* are chosen as specified in §3.3.2.

REFERENCES

- ÅKERVIK, E., EHRENSTEIN, U., GALLAIRE, F. & HENNINGSON, D. S. 2008 Global two-dimensional stability measures of the flat plate boundary layer flow. *Eur. J. Mech B* **27**, 501–513.
- ANDERSSON, P., BERGGREN, M. B. & HENNINGSON, D. S. 1999 Optimal disturbances and bypass transition in boundary layers. *Phys. Fluids* **11**, 134–150.
- ANDERSSON, P., HENNINGSON, D. S. & HANIFI, A. 1998 On a stabilization procedure for the parabolic stability equations. *J. Engng Math.* **33** (3), 311–332.
- BAGHERI, S. & HANIFI, A. 2007 The stabilizing effect of streaks on Tollmien–Schlichting and oblique waves: a parametric study. *Phys. Fluids* **19**, 078103.
- BERTOLOTTI, F. P., HERBERT, T. & SPALART, P. R. 1992 Linear and nonlinear stability of the Blasius boundary layer. *J. Fluid Mech.* **242**, 441–474.
- BIPPES, H. 1999 Basic experiments on transition in three-dimensional boundary layers dominated by crossflow instability. *Progr. Aerosp. Sci.* **35**, 363–412.
- BREUER, K. S. & KURAISHI, T. 1994 Transient growth in two- and three-dimensional boundary layers. *Phys. Fluids* **6** (6), 1983–1993.
- BUTLER, K. M. & FARRELL, B. F. 1992 Three-dimensional optimal perturbations in viscous shear flow. *Phys. Fluids* **4**, 1637–1650.
- BYSTRÖM, M. G. 2007 Optimal disturbances in boundary layer flows. Licentiate thesis, KTH, Stockholm.
- CHAPMAN, S. J., LAWRY, J. M. H. H., OCKENDON, J. R. & TEW, R. H. 1999 On the theory of complex rays. *SIAM Rev.* **41** (3), 417–509.
- COOKE, J. C. 1950 The boundary layer of a class of infinite yawed cylinders. *Proc. Camb. Phil. Soc.* **46**, 645–648.
- CORBETT, P. & BOTTARO, A. 2000 Optimal perturbations for boundary layers subject to streamwise pressure gradient. *Phys. Fluids* **12** (1), 120–130.
- CORBETT, P. & BOTTARO, A. 2001 Optimal linear growth in swept boundary layers. *J. Fluid Mech.* **435**, 1–23.
- DEYHLE, H. & BIPPES, H. 1996 Disturbance growth in an unstable three-dimensional boundary layer and its dependence on environmental conditions. *J. Fluid Mech.* **316**, 73–113.
- ELLINGSEN, T. & PALM, E. 1975 Stability of linear flow. *Phys. Fluids* **18** (4), 487–488.
- GRÉA, B. J., LUCHINI, P. & BOTTARO, A. 2005 Ray theory of flow instability and the formation of caustics in boundary layers. IMFT Technical Report 2005-1.
- HAJ-HARIRI, H. 1994 Characteristics analysis of the parabolized stability equations. *Stud. Appl. Math.* **92**, 41–53.
- HANIFI, A., HENNINGSON, D. S., HEIN, S., BERTOLOTTI, F. P. & SIMEN, M. 1994 Linear non-local instability analysis – the linear NOLOT code. FFA Technical Report FFA TN 1994-54.
- HANIFI, A., SCHMID, P. J. & HENNINGSON, D. S. 1996 Transient growth in compressible boundary layer flow. *Phys. Fluids* **8** (3), 826–837.
- HENNINGSON, D. S., LUNDBLADH, A. & JOHANSSON, A. 1993 A mechanism for bypass transition from localized disturbances in wall-bounded shear flows. *J. Fluid Mech.* **250**, 169–238.
- HERBERT, T. 1997 Parabolized stability equations. *Annu. Rev. Fluid Mech.* **29**, 245–283.

- HÖGBERG, M. & HENNINGSON, D. 1998 Secondary instability of crossflow vortices in Falkner–Skan–Cooke boundary layers. *J. Fluid Mech.* **368**, 339–357.
- HULTGREN, L. & GUSTAVSSON, L. 1981 Algebraic growth of disturbances in a laminar boundary. *Phys. Fluids* **24** (6), 1000–1004.
- KENDALL, J. M. 1985 Experimental study of disturbances produced in a pre-transitional laminar boundary layer by weak free-stream turbulence. *Paper* 85-1695. AIAA.
- KLEBANOFF, P. S. 1971 Effect of free-stream turbulence on the laminar boundary layer. *Bull. Am. Phys. Soc.* **10**, 1323.
- LANDAHL, M. T. 1980 A note on algebraic instability of inviscid parallel shear flows. *J. Fluid Mech.* **98**, 243–251.
- LEVIN, O. & HENNINGSON, D. S. 2003 Exponential vs algebraic growth and transition prediction in boundary layer flow. *Flow Turbul. Combust.* **70**, 183–210.
- LI, F. & MALIK, M. R. 1996 On the nature of the PSE approximation. *Theoret. Comput. Fluid Dyn.* **8**, 253–273.
- LI, F. & MALIK, M. R. 1997 Spectral analysis of parabolized stability equations. *Comp. Fluids* **26** (3), 279–297.
- LUCHINI, P. 2000 Reynolds-number-independent instability of the boundary layer over a flat surface: optimal perturbations. *J. Fluid Mech.* **404**, 289–309.
- MATSUBARA, M. & ALFREDSSON, P. H. 2001 Boundary-layer transition under free-stream turbulence. *J. Fluid Mech.* **430**, 149–168.
- ORR, W. M. F. 1907 The stability or instability of the steady motions of a liquid. *Proc. R. Irish Acad. A* **27**, 9–69.
- PRALITS, J. O., AIRIAU, C., HANIFI, A. & HENNINGSON, D. S. 2000 Sensitivity analysis using adjoint parabolized stability equations for compressible flows. *Flow Turbul. Combust.* **65**, 321–346.
- PRALITS, J. O., BYSTRÖM, M. G., HANIFI, A., HENNINGSON, D. S. & LUCHINI, P. 2007 Optimal disturbances in three-dimensional boundary-layer flows. *Ercoftac Bull.* **74**, 23–31.
- REDDY, S. C. & HENNINGSON, D. S. 1993 Energy growth in viscous channel flow. *J. Fluid Mech.* **252**, 209–238.
- SARIC, W. S., REED, H. L. & WHITE, E. B. 2003 Stability and transition of three-dimensional boundary layers. *Annu. Rev. Fluid Mech.* **35**, 413–440.
- SCHLICHTING, H. 1979 *Boundary-Layer Theory*, 17th edn. McGraw-Hill.
- SCHMID, P. J. & HENNINGSON, D. S. 2001 *Stability and Transition in Shear Flows*. Springer.
- SCHRADER, L. U., AMIN, S. & BRANDT, L. 2010 Transition to turbulence in the boundary layer over a smooth and rough swept plate exposed to free-stream turbulence. *J. Fluid Mech.* **646**, pp. 297–325.
- SCHRADER, L. U., BRANDT, L. & HENNINGSON, D. S. 2009 Receptivity mechanisms in three-dimensional boundary layer flows. *J. Fluid Mech.* **618**, 209–241.
- SIMEN, M. 1992 Local and non-local stability theory of spatially varying flows. In *Instability, Transition and Turbulence* (ed. M. Y. Hussaini, A. Kumar & C. L. Streett), pp. 181–195. Springer.
- TUMIN, A. & RESHOTKO, E. 2003 Optimal disturbances in compressible boundary layers. *Paper* 2003-0792. AIAA.